12-2018

H₂ Oxidation Over Supported Au Nanoparticle Catalysts: Evidence for Heterolytic H₂ Activation at the Metal-Support Interface

Todd N. Whittaker
Trinity University, twhittak@trinity.edu

K. B. Sravan Kumar
Trinity University

Christine Peterson
Trinity University, cpeters4@trinity.edu

Meagan N. Pollock
Trinity University, mpollock@trinity.edu

L. C. Grabow

See next page for additional authors

Repository Citation

Authors

Todd N. Whittaker, K. B. Sravan Kumar, Christine Peterson, Meagan N. Pollock, L. C. Grabow, and Bert D. Chandler

H$_2$ Oxidation over Supported Au Nanoparticle Catalysts: Evidence for Heterolytic H$_2$ Activation at the Metal−Support Interface

Todd Whittaker,[†,§] K. B. Sravan Kumar,[‡,§] Christine Peterson,[†] Meagan N. Pollock,[†] Lars C. Grabow,[‡] and Bert D. Chandler*[†]

[†]Department of Chemistry, Trinity University, San Antonio, Texas 78212-7200, United States

[‡]Department of Chemical and Biomolecular Engineering, University of Houston, Houston, Texas 77204-4004, United States

S *Supporting Information*

ABSTRACT: Water adsorbed at the metal−support interface (MSI) plays an important role in multiple reactions. Due to its importance in CO preferential oxidation (PrOx), we examined H$_2$ oxidation kinetics in the presence of water over Au/TiO$_2$ and Au/Al$_2$O$_3$ catalysts, reaching the following mechanistic conclusions: (i) O$_2$ activation follows a similar mechanism to that proposed in CO oxidation catalysis; (ii) weakly adsorbed H$_2$O is a strong reaction inhibitor; (iii) fast H$_2$ activation occurs at the MSI, and (iv) H$_2$ activation kinetics are inconsistent with traditional dissociative H$_2$ chemisorption on metals. Density functional theory (DFT) calculations using a supported Au nanorod model suggest H$_2$ activation proceeds through a heterolytic dissociation mechanism, resulting in a formal hydride residing on the Au and a proton bound to a surface TiOH group. This potential mechanism was supported by infrared spectroscopy experiments during H$_2$ adsorption on a deuterated Au/TiO$_2$ surface, which showed rapid H−D scrambling with surface hydroxyl groups. DFT calculations suggest that the reaction proceeds largely through proton-mediated pathways and that typical Brønsted−Evans Polanyi behavior is broken by introducing weak acid/base sites at the MSI. The kinetics data were successfully reinterpreted in the context of the heterolytic H$_2$ activation mechanism, tying together the experimental and computational evidence and rationalizing the observed inhibition by physiorbed water on the support as blocking the MSI sites required for heterolytic H$_2$ activation. In addition to providing evidence for this unusual H$_2$ activation mechanism, these results offer additional insight into why water dramatically improves CO PrOx catalysis over Au.
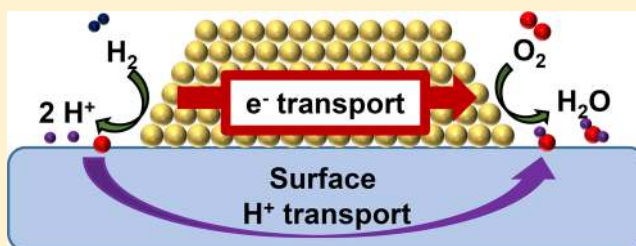
INTRODUCTION

The global chemical industry produces over 50 million tons of hydrogen for several important processes including ammonia and methanol synthesis, petroleum refining, and hydrogenation reactions.[1,2] Industrial H$_2$ production (predominantly by methane steam reforming and water−gas shift units) results in H$_2$ feeds containing about 1% CO. Many downstream uses of H$_2$, particularly ammonia synthesis catalysts and fuel cells, are highly sensitive to CO, so it must be removed. The scale of hydrogen production and the potential for preparing fuel cell grade hydrogen make hydrogen purification an enormously impactful process: ammonia production in particular accounts for ∼3% of total global energy consumption.[3] Methanation (CO + 3H$_2$ → CH$_4$ + H$_2$O) and pressure swing adsorption are currently used to purify H$_2$, but each method has its limitations.[2]

Another option for hydrogen purification is the preferential oxidation of CO with O$_2$ (PrOx reaction). In PrOx, a small amount of O$_2$ (typically ∼1%) is added to the feed; the goal is to find catalysts that can oxidize all of the CO without oxidizing any H$_2$. A typical benchmark goal for this reaction is to reduce the CO concentration at the reactor outlet to 50 ppm with O$_2$ selectivity to CO$_2$ ≥ 50%.[4−6] This places enormous selectivity demands on the catalyst, which must oxidize CO ∼10^6 times faster than H$_2$. Supported Au nanoparticle catalysts are notoriously slow hydrogenation catalysts,[7] yet are highly active for CO oxidation;[8−13] thus, they should be well-suited for the CO PrOx reaction.

Several research groups have investigated CO PrOx over Au in the past two decades,[5,14−21] with mechanistic studies performed by the Behm[5,14−17] and Piccolo and Rousset groups,[18,19] as well as computational investigations by Mavrikakis and co-workers.[20,21] In most cases, the presence of H$_2$ was found to increase CO oxidation activity. Water plays an important role as a co-catalyst in CO oxidation,[13,22−29] so these observations are consistent with the in-situ production of water. Early studies by Behm showed water to improve CO PrOx performance by suppressing H$_2$ oxidation and at least partially prevent carbonate poisoning.[14]

We recently showed that PrOx performance can be dramatically improved by orders of magnitude when the surface coverage of physisorbed water is controlled.[30] This improvement was greater than expected based on weakly adsorbed water's role as a co-catalyst in CO oxidation.[13,31] In order to better understand the performance-enhancing ability

of water, we undertook a more detailed examination of effects of weakly adsorbed water on the undesirable half of the PrOx reaction: H_2 oxidation. Our reaction kinetics study, carried out at low conversions, indicates that H_2 coverage is rate limiting and that physisorbed water is a strong inhibitor for the reaction. Both kinetics data and density functional theory (DFT) calculations indicate that H_2 is selectively activated at the metal support interface (MSI) and suggest that the water inhibition is primarily due to the physical blocking of these MSI sites.

The reaction kinetics, DFT results, and supporting infrared spectroscopic characterization of H_2 adsorption on a D_2O-exchanged catalyst indicate that H_2 oxidation occurs at the MSI through a heterolytic H_2 activation pathway. This is a surprising discovery. Hydrogen adsorption and activation is one of the most studied reactions in all of chemistry; early investigations into the interactions between hydrogen and various metals date back to the mid-19th century.[32−34] Hydrogenation reactions over heterogeneous catalysts are widely used in industry and have been studied for over a century.[35−38] Similarly, the mechanism of hydrogen activation by inorganic complexes, dating back to seminal work by Wilkinson and Vaska, has been widely studied for more than 50 years.[39] The overwhelming majority of these studies show that hydrogen activation occurs via similar mechanisms: oxidative addition for transition metal complexes[40,41] and (homolytic) dissociative chemisorption for metals and supported metal catalysts.[42,43]

There are exceedingly few reports of heterolytic H_2 activation by heterogeneous catalysts; Coperet's work on Al_2O_3 defect sites provides several notable examples,[44−46] and Boudart proposed such a mechanism at paramagnetic centers of MgO.[47] Examples of heterolytic H_2 activation are well-known in biological systems, particularly hydrogenase enzymes and their synthetic models.[48,49] Recent studies on frustrated Lewis pairs (FLPs) show similar H_2 reaction pathways.[50−53] The studies reported herein provide strong evidence that supported metal nanoparticle catalysts can also operate via similar Lewis acid−base mechanisms, highlighting the mechanistic similarities between biological, homogeneous, and heterogeneous catalysts.

EXPERIMENTAL SECTION

Materials. Gases (H_2, N_2, O_2, 20 vol % O_2/He, and 5 vol % CO/He) were 5.0 grade supplied by Praxair and used without further purification. Water was purified to a resistivity of 18.2 MΩ with a Barnstead Nanopure System; no additional purification methods were employed. Commercial catalysts were purchased from STREM Chemicals. The catalysts have been fully characterized elsewhere;[54] briefly, the catalysts were nominally 1 wt % Au, and the particle sizes were 2.9 ± 0.9 and 2.2 ± 0.7 nm for Au/TiO_2 and Au/Al_2O_3, respectively The TiO_2 was P25 and the Al_2O_3 was γ-Al_2O_3. SiC (400 mesh) was purchased from Sigma-Aldrich.

Reactor System. The H_2 oxidation reactor consisted of a home-built laboratory-scale single-pass plug-flow microreactor operated at atmospheric pressure (760 Torr). Gas flows were controlled with four electronic low-pressure mass flow controllers (Porter Instruments). Water was added to the feed using a two-stage water saturator after the reactant gases were mixed; feedwater pressure was determined by adjusting the temperature of the second stage. The composition of the feed and reactor effluent (CO, CO_2, and O_2) was determined using a Siemens Ultramat 23 IR gas analyzer with electrochemical O_2 sensor. The feed concentration was determined via a reactor bypass loop. The reaction zone consisted of finely ground fresh catalyst (5−100 mg)

diluted in 1 g of SiC. The catalyst powder was mixed thoroughly with the SiC and finely chopped using a spatula until homogeneous.

Immediately prior to kinetics experiments, the diluted catalyst was pretreated in a mixture of 10 vol % H_2, 10 vol % O_2, and balance N_2 at 100 °C for 1 h. This treatment was employed to ensure a consistent degree of surface hydroxylation on the catalyst and to remove impurities (e.g., surface organics, carbonates). The reactor was then cooled to the reaction temperature under flowing gas consisting of 19 Torr of H_2O/N_2. The system was allowed to equilibrate for 30 min at constant reactor and water saturator temperature whenever the H_2O pressure was changed. The catalyst water coverage was calculated from volumetric H_2O adsorption isotherms.[30]

H_2 Oxidation Kinetics. Conversions were measured 5 min after steady state was achieved by collecting gas composition data every 10 s for 2 min. Steady state was defined as O_2 slip being constant with a range of 0.02 vol % O_2 over 5 min. During kinetic experiments, conversions were held below 15% in order to maintain differential reaction conditions and keep H_2O generation low with respect to the added H_2O. Gases (3−60 vol % H_2, 0.9−10 vol % O_2 with 5−18 Torr H_2O added via saturator) were fed to the reactor at weight hourly space velocities (WHSVs) of $(0.2−2.3) \times 10^3$ L/g_{cat}/h. The reaction temperature was 60 °C. H_2O reaction orders were measured with 60 vol % H_2 and 1 vol % O_2. O_2 reaction orders were measured with 60 vol % H_2 at three different H_2O pressures (6.8, 11, and 18 Torr). H_2 reaction orders were measured with 10 vol % O_2 at four different H_2O pressures (5, 6, 9, and 12 Torr).

DFT Calculations. Plane wave based density functional theory (DFT) calculations with periodic boundary conditions were performed using the Vienna Ab Initio Simulation Package (VASP).[55−57] Exchange and correlation were described with the BEEF-vdW functional,[58] and the projector augmented wave (PAW) method was used to approximate the core electronic structure.[59,60] Spin polarization was used wherever necessary, i.e., the adsorption and activation of O_2. A plane wave energy cutoff of 400 eV was used for all the calculations. The same energy cutoff of 400 eV was used previously for studying CO oxidation on Au/TiO_2.[61] The gas phase H_2 and H_2O energies were calculated in a $10 \times 10 \times 10$ Å simulation box, and Brillouin zone sampling was restricted to the Γ point. For gas phase species, we employed a Gaussian smearing with $k_bT = 0.01$ eV, and geometries were optimized using a force convergence criterion of 0.01 eV/Å.

For bulk and slab models, we employed Gaussian smearing with a Fermi temperature of $k_bT = 0.1$ eV, and the total energy was extrapolated to $k_bT = 0.0$ eV. Residual forces on equilibrium geometries were converged to below 0.05 eV/Å. The reaction energy for the bulk oxidation from Ti_2O_3 to TiO_2 was reproduced within an error of 0.04 eV with this arrangement; consequently, implementation of the DFT+U approach by Dudarev et al. was not necessary.[62,63] The computationally optimized lattice constants are $a = 4.654$ Å, $a/c = 1.561$ for TiO_2 and $a = 4.223$ Å for Au. These values agree well with experimentally observed lattice constants of $a = 4.682$ Å, $a/c = 1.574$ for TiO_2,[64] and $a = 4.08$ Å for Au.[65] For slab models, we used a $3 \times 2 \times 1$ Monkhorst−Pack k-point mesh to sample the Brillouin zone, and a dipole correction was applied to the electrostatic potential in the z direction.

Transition states were located using the climbing image nudged elastic band (NEB) method and refined as necessary with the dimer method with a convergence criterion of 0.1 eV/Å. All transition states were confirmed as true saddle points with a single imaginary frequency mode along the reaction coordinate. Vibrational frequencies were obtained using the atomic simulation environment (ASE) module in the harmonic oscillator approximation with a displacement of 0.01 Å along each positive and negative Cartesian direction. Atomic charges were estimated based on a Bader analysis.[66−68]

Au/TiO_2 Computational Model. The basis for the Au/TiO_2 interface is formed by a rutile TiO_2(110) (5×3) unit cell separated by 20 Å of vacuum space in the z direction perpendicular to the surface. The bottom two bilayers of TiO_2 were fixed in their bulk positions, while all other degrees of freedom were relaxed. We did not
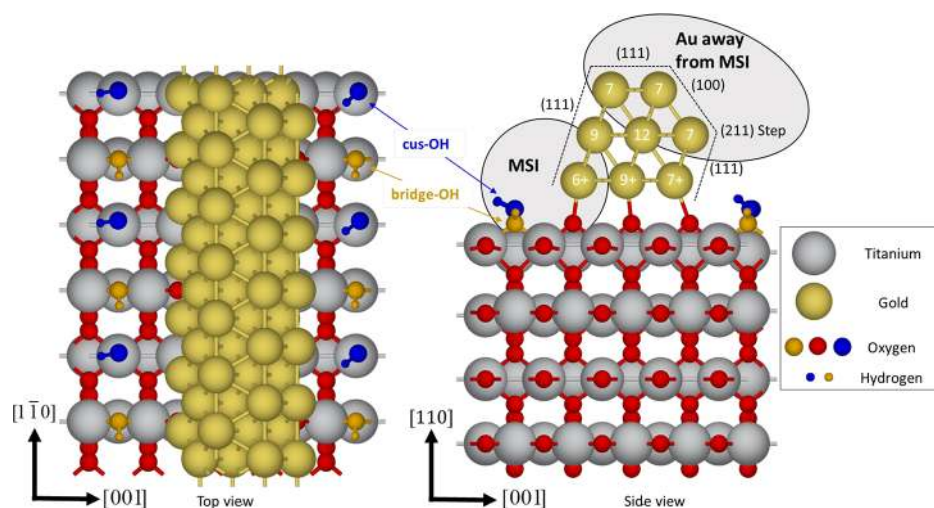
Figure 1. Side and top views of the Au/TiO$_2$ interface model using atomic radii. Two types of hydroxyl groups are differentiated by color with cus-OH shown in blue and bridge-OH in orange. In the side view, the terminating surfaces of the Au rod are labeled and the coordination numbers for each atom are indicated in white. The general regions referred to as MSI and Au atoms away from the MSI are highlighted.

consider oxygen vacancies on the TiO$_2$ surface because the presence of significant amounts of O$_2$ and H$_2$O in the experimental feed is likely to heal or passivate surface defects quickly.[69] Next, a three-layer gold nanorod was placed along the [1$\overline{1}$0] direction of TiO$_2$ with its (111) facet exposed at the interface. We refer to this model as Au(111)/TiO$_2$(110). The lattice constant mismatch between Au and TiO$_2$ was minimized with a nanorod length of seven Au atoms, leaving a residual compressive strain of 5.53% in the Au nanorod along the [1$\overline{1}$0] direction of the TiO$_2$ unit cell. A similar level of strain was reported by Henkelman et al. with the gold nanorod oriented in the [1$\overline{1}$0] direction.[61] Compressive strain is known to lower the d-band center of metals and, in turn, decrease their reactivity.[70] We have quantified the effect of 5.53% compressive strain on H$_2$ dissociation on Au(211) step sites in the Supporting Information (SI). These estimates indicate that compressive strain alters the activation energies by less than 0.07 eV and the dissociation energies by only 0.02 eV. We consider this error negligible within the context of our study, and our qualitative conclusions are robust with respect to the effect of strain.

The Au nanorod model on TiO$_2$ used in this study has been improved from previous nanorod models[11,61,71] to accommodate possible sites for H$_2$ activation and allow for comparisons between reactions on the metal and at the MSI. The effect of surface hydroxylation was approximated by creating bridge-hydroxyl groups (bridge-OH) at all available bridging oxygens on the TiO$_2$ surface and hydroxyl groups at coordinatively unsaturated (cus) Ti atoms (cus-OH). The hydroxylation state of the Au/TiO$_2$ model shown in Figure 1 can also be thought of as a model having a monolayer equivalent (MLE) of dissociated water molecules on the exposed TiO$_2$ surface. When comparing reaction energetics between Au sites away from the MSI to activity near or at the MSI, we refer to sites within the highlighted regions of Figure 1. The Au sites are composed of atoms in local (111), (100), and (211) geometries and have a coordination number (CN) of 7. The edge atoms at the MSI have a CN of 6+, where 6 strictly counts Au neighbors and "+" accounts for bonds made with the TiO$_2$ support. As we demonstrate in the Results and Discussion section, the activation barrier for homolytic H$_2$ activation at these Au$_{MSI}$ sites with CN = 6+ is in fact slightly higher than on the (211)-type Au sites with CN = 7. Thus, the small difference in coordination number alone cannot account for a large difference in reactivity when interfacial reactions are studied.

FTIR Spectroscopy. FTIR spectra during H$_2$ adsorption were collected on a Thermo Nicolet Nexus 470 FTIR spectrometer in a heated (20−300 °C) transmission flow cell. H$_2$O in the feed gases was removed by a dry ice−iso-propyl alcohol (IPA) moisture trap. For the exchange experiment, 30 mg of catalyst sample was pressed (5 tons of pressure for 1 min) in a 13 mm circular pellet, which was mounted in

the flow cell. D$_2$O (99.0%, Cambridge Isotope Laboratories) was flowed through the pellet for 30 min using a two-stage saturator. The complete deuteration of the support was monitored by collecting scans over the course of the treatment. The weakly adsorbed D$_2$O was removed by flowing N$_2$ at 120 °C for 1 h before cooling to 70 °C. This ensured no weakly adsorbed D$_2$O remained and only OD and strongly adsorbed D$_2$O were present. H$_2$ was then flowed over the catalyst at a WHSV of 40 L/g$_{cat}$/h for 30 min, with scans collected every 5 min.

RESULTS AND DISCUSSION

Kinetic measurements on CO oxidation have been previously reported;[13,31] these studies showed that weakly adsorbed H$_2$O plays a number of important mechanistic roles during CO oxidation. Protons from water help to activate O$_2$ by generating Au-OOH, which quickly reacts with CO, yielding Au-COOH. Physisorbed water also plays a role in the rate-determining decomposition of Au-COOH, acting as a proton acceptor as the catalyst releases CO$_2$. During PrOx, the primary feed component is H$_2$ and some (undesirable) H$_2$ oxidation occurs.[30] Note that Behm has demonstrated that CO and H$_2$ compete for the same O intermediate in PrOx, so understanding H$_2$ activation may help to understand and control this competition.[16] Goodman's work used inelastic neutron scattering experiments to characterize a reactive O species during H$_2$ oxidation as an −OOH species on Au.[72] We therefore aim to understand water's role in H$_2$ oxidation for both fundamental and practical reasons.[14]

Reaction Kinetics. Figure 2 shows how added water affects H$_2$ oxidation under typical PrOx conditions (1 vol % O$_2$, 60 vol % H$_2$, 60 °C, 50 mg of catalyst); the data clearly show that H$_2$O inhibits H$_2$ oxidation. Water is the reaction product, so under PrOx conditions, the water produced from the reaction impacts the reaction kinetics. The red diamonds in Figure 2A show the total amount of water in the system, including the water produced from H$_2$ oxidation calculated from the O$_2$ conversion data. Under these conditions, in-situ water production is greater than the H$_2$O added to the system.

The strong inhibitory effect of water complicates these measurements because the total water pressure in the system (including the water produced by the reaction) must be held approximately constant for a given measurement. Total O$_2$
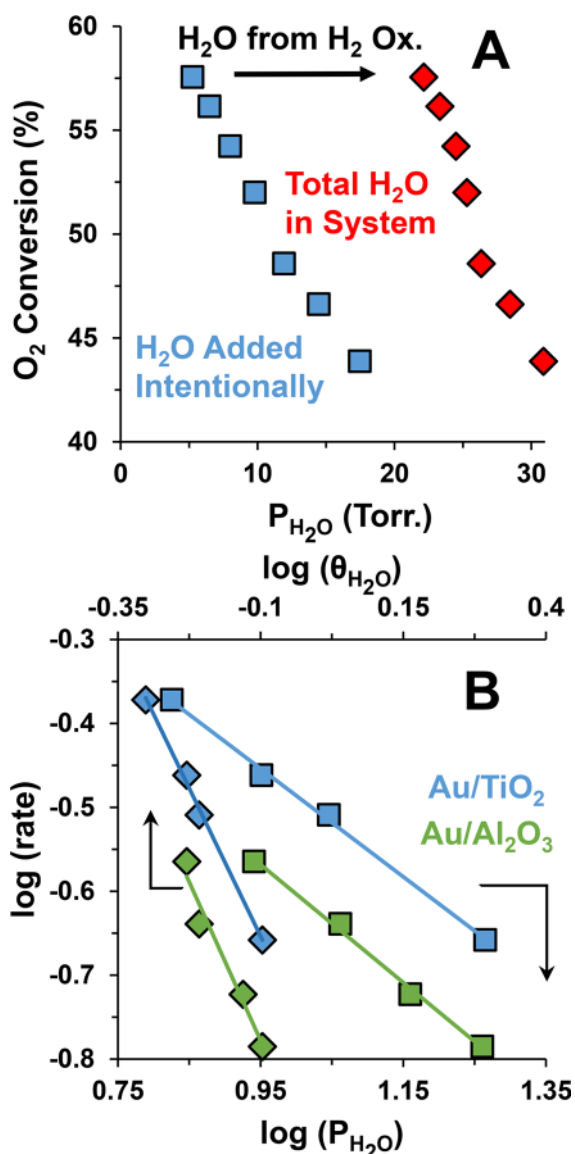
Figure 3. Hydrogen reaction order plots for Au/Al_2O_3 (green circles, 6.4 Torr H_2O, 60 °C) and Au/TiO_2 (blue squares, 6.4 Torr H_2O, 60 °C).

Figure 2. Effects of added water on H_2 oxidation. (A) O_2 conversion as a function of H_2O pressure. The blue squares represent the amount of H_2O vapor intentionally added to the feed. The red diamonds represent the total amount of H_2O in the reactor effluent (intentionally added H_2O plus H_2O generated from reaction). Reaction conditions: 1 wt % Au/Al_2O_3 catalyst, 60 °C, 60 vol % H_2, 1 vol % O_2, WHSV: 216 $L/g_{cat}/h$. (B) H_2O reaction order plots for Au/TiO_2 (blue) and Au/Al_2O_3 (green) at 60 °C under differential reaction conditions. The squares present the data plotted against $\log(P_{H_2O})$; the diamonds present the same data plotted against $\log(\theta_{H_2O})$. Reaction conditions: 60 vol % H_2, 1 vol % O_2, WHSV: 1080 $L/g_{cat}/h$. Rate units were $mol_{H_2O}/mol_{Au}/s$; pressure units were Torr.

conversions were held below 15% to maintain differential reactor conditions; additionally, the amount of water generated from the reaction was small relative to the amount of water intentionally added (<5 vol % for high water pressures and <25 vol % at the lowest water pressure). This puts significant constraints on the reactor operating conditions, requiring water coverages of >0.5.

Figure 2B shows kinetic data for Au/Al_2O_3 and Au/TiO_2; the extracted H_2O reaction orders are −0.70 and −0.64,
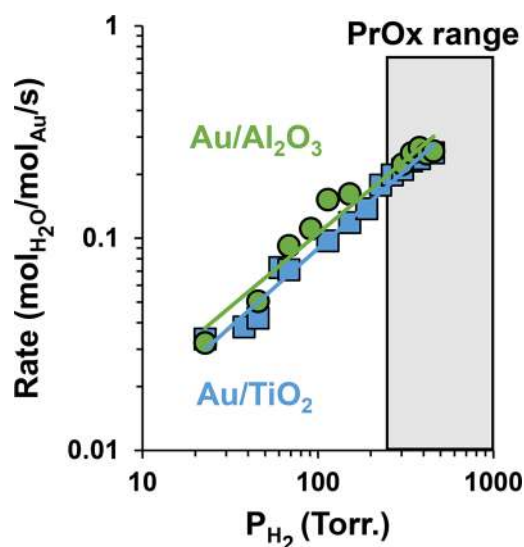
respectively. It is important to clarify that we previously identified weakly bound or physisorbed water as the mechanistically important proton donor in O_2 activation over both Au/TiO_2 and Au/Al_2O_3 catalysts.[13,73] Any strongly bound water, e.g., to exposed Ti atoms, is unlikely to be sufficiently mobile to participate in the fast proton donation associated with O_2 activation (and Au-COOH decomposition in CO oxidation). Further, the water pressures and reaction temperatures used in the current study affect the amount of water physisorbed on the support hydroxyl groups. Therefore, equilibrium adsorption isotherm measurements for water on the two catalysts were used to estimate the surface coverage of weakly adsorbed water (θ_{H_2O}). While this is an imperfect comparison relative to the flow system, the errors introduced are partially compensated by the additional water produced from the reaction. Further, errors in the coverage estimates are inherently included in the overall errors associated with the rate measurements. Figure 2B shows the water dependence data plotted with respect to θ_{H_2O}. The fits are quite good, indicating that any errors in the estimation of θ_{H_2O} are not likely to have a significant influence on the results. The reaction orders with respect to θ_{H_2O} are about −1.5, further showing the strong inhibition of H_2 oxidation by weakly adsorbed water.

Figure 3 shows the H_2 pressure dependence data over a large range of H_2 pressures (1−60 vol %); Figure 4 shows H_2 order plots at different water pressures. The extracted reaction orders for H_2, O_2, and H_2O are compiled in Table 1 and compared to the kinetic data for CO oxidation. Hydrogen oxidation is approximately first order in H_2, suggesting that H_2 activation is a kinetically important step. As Table 1 shows, the key difference between CO and H_2 oxidation is the water dependence: weakly adsorbed water promotes CO oxidation but inhibits H_2 oxidation. Since weakly adsorbed water is required for fast O_2 activation, this suggests that the same physisorbed water inhibits H_2 activation. Water does not adsorb to Au under these conditions,[74] and the physisorbed water resides on the support. Therefore, if physisorbed water

Table 1. Summary of Reaction Orders during H_2 and CO Oxidation Catalysis

Reactant	P_{H_2O} (Torr.)	H_2 Oxidation		CO Oxidation	
		Au/TiO$_2$	Au/Al$_2$O$_3$	Au/TiO$_2$	Au/Al$_2$O$_3$
H_2[a]	12	0.60 ± 0.06	0.90 ± 0.10	---	---
	9	0.58 ± 0.06	0.77 ± 0.09		
	6	0.70 ± 0.08	0.92 ± 0.07		
	5	0.66 ± 0.06	0.74 ± 0.05		
CO[b]	1	---	---	0^{13}	0^{30}
O_2[c]	18.2	0.21 ± 0.01	0.37 ± 0.09	0.21^{13}	0.35^{30}
	10.8	0.12 ± 0.01	0.29 ± 0.08		
	6.4	0.28 ± 0.07	0.40 ± 0.10		
H_2O[d]		-0.64 ± 0.02	-0.70 ± 0.03	0.33^{13}	0.35^{13}
		-1.41 ± 0.06	-1.5 ± 0.2	1.33^{13}	1.82^{13}

[a]H_2 (3–20 vol %), O_2 (10 vol %), H_2O (12, 9, 6, 5 Torr), 60 °C, WHSV = 2.3×10^3 L/g$_{cat}$/h. [b]CO (0.56–1.4 vol %), O_2 (20 vol %), H_2O (0.001, 0.5 Torr), 20 °C, WHSV = 2.2×10^3 L/g$_{cat}$/h. [c]H_2 (60 vol %), O_2 (0.9–2.1 vol %), H_2O (18.2, 10.8, 6.8 Torr), 60 °C, WHSV = 2.3×10^3 L/g$_{cat}$/h. [d]H_2 (60 vol %), O_2 (1 vol %), H_2O (6.8–18.2 Torr), 60 °C, WHSV = 2.3×10^3 L/g$_{cat}$/h. The top row reports the water reaction order relative to the gas phase water pressure (P_{H_2O}); the bottom row reports the reaction order relative to the surface water coverage (θ_{H_2O}).
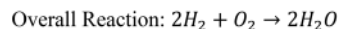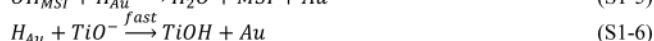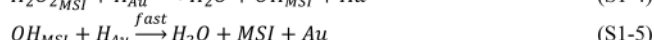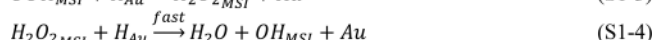
inhibits hydrogen activation, this process most likely occurs at the MSI.

Traditional Models for Hydrogen Activation on Metals. The widely accepted mechanism for H_2 adsorption/ activation on metals (Pt, Pd, Rh, Ru, Ni, etc.) involves H_2 adsorption and homolytic H–H bond cleavage, yielding two surface H atoms (dissociative chemisorption).[75−81] This process is largely equivalent to the classic mechanism of oxidative addition on transition metal complexes. In both cases, H_2 dissociation formally oxidizes the nanoparticle by two electrons, and the adsorbed H atoms can be considered formal hydrides from an electron-counting perspective, even if the bonding is largely covalent and there is relatively little charge separation. We note that this distinction and nomenclature is primarily used in order to carefully account for all of the protons and electrons in the system. Dissociative chemisorption or oxidative addition is therefore considered to generate surface hydrogen atoms and hydrides, respectively; this treatment essentially equates these two limiting species. The key distinction we wish to make is between a proton and a hydride/hydrogen atom. Since "hydrogen atom" is often used ambiguously, we refer to Au-H species as formal hydrides. This general mechanism is presented in eq 1:

$$H_2 + 2M \overset{K_{H_2}}{\rightleftharpoons} 2H_M \qquad (1)$$

The traditional mechanism is difficult to reconcile with the kinetic data, particularly (i) the inhibition by weakly adsorbed water, (ii) additional analysis of the kinetic data (see below), and (iii) previous H_2-D_2 equilibration studies. It is difficult to rationalize the water inhibition data above if the entire metal surface participates in H_2 activation. The van der Waals interactions between Au and water are so weak that Au is considered to be essentially hydrophobic,[82−84] and water adsorption on Au surfaces is only observed at very low temperatures.[85−89] In comparison, water readily engages in hydrogen-bonding interactions with support hydroxyl groups during physisorption. Further, our previous volumetric and infrared spectroscopic water adsorption studies are consistent with water adsorption on the support rather than the Au.[30] Haruta's H_2−D_2 equilibration studies also suggested that H_2 activation is site-specific, occurring at the MSI.[90]

Scheme 1. Elementary Steps for H_2 Oxidation on Au via Homolytic H_2 Activation on Au Sites Away from the MSI[a]

$$MSI + O_2 + TiOH \overset{K_{O_2}}{\rightleftharpoons} OOH_{MSI} + TiO^- \qquad (S1-1)$$

$$2(2Au + H_2 \overset{k_2}{\rightarrow} 2H_{Au}) \qquad (S1-2)$$

$$OOH_{MSI} + H_{Au} \overset{k_3}{\rightarrow} H_2O_{2MSI} + Au \qquad (S1-3)$$

$$H_2O_{2MSI} + H_{Au} \overset{fast}{\longrightarrow} H_2O + OH_{MSI} + Au \qquad (S1-4)$$

$$OH_{MSI} + H_{Au} \overset{fast}{\longrightarrow} H_2O + MSI + Au \qquad (S1-5)$$

$$H_{Au} + TiO^- \overset{fast}{\longrightarrow} TiOH + Au \qquad (S1-6)$$

Overall Reaction: $2H_2 + O_2 \rightarrow 2H_2O$

[a]"MSI" sites are Au atoms at the metal support interface, Au sites are considered to be away from the MSI, and TiOH sites are support hydroxyl groups. Steps S1-2 and S1-3 are both considered to be kinetically important; all subsequent steps are considered fast.

Double-reciprocal (e.g., Lineweaver–Burk) plots, which, in this case, graph 1/rate vs $1/P_{H_2}$, can be useful in evaluating changes to heterogeneous catalysts.[13,91−96] When coupled with appropriate kinetic models, double reciprocal plots can provide a useful framework for evaluating the viability of a reaction mechanism, the intrinsic activity at an active site, and a means of evaluating changes to the number of active sites on a catalyst. Hydrogen oxidation over Au is generally described as limited by hydrogen activation in the literature.[97,98] Homolytic H_2 activation on the Au surface and subsequent reaction with Au-OOH at the MSI can be considered with a kinetic model similar to the H_2 oxidation mechanism on Pt proposed by Dumesic and co-workers. This mechanism involves hydrogen activation on the metal followed by reaction with an activated oxygen species (see Scheme 1).[80]

Applying the steady state approximation, which also assumes a constant coverage of Au-OOH at a particular water pressure, yields the following rate law in eq 2 (full derivation available in the SI):

$$\nu_{homo} = \frac{k_3 k_2 P_{H_2}^{0.5} K'_{O_2} P_{O_2} [Au]_T [MSI]_T}{k_3 K'_{O_2} P_{O_2} [MSI]_T + k_2 P_{H_2}^{0.5} (1 + K'_{O_2} P_{O_2})} \qquad (2)$$
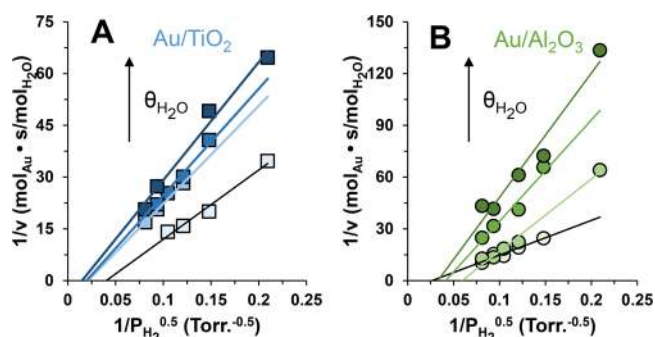
Figure 5. Hydrogen dependence data (Figure 4) fit to eq 3 for (A) Au/TiO$_2$ and (B) Au/Al$_2$O$_3$.

$$K_R = \frac{\text{slope}}{\text{intercept}} = \frac{k_3}{k_2}\left(\frac{K'_{O_2}P_{O_2}}{1 + K'_{O_2}P_{O_2}}\right)[\text{MSI}]_T \tag{5}$$

Figure 5 shows the H$_2$ dependence data (Figure 4) fitted to eq 3. While the data are reasonably linear, all of the lines have y-intercepts < 0, implying physically meaningless negative values for the extractable kinetic parameters (v_{max}, K_R). Thus, the traditional homolytic H$_2$ adsorption model, where the rate-determining step is either homolytic H$_2$ adsorption or the reaction of the adsorbed Au-H with an adsorbed O species, is inconsistent with the kinetic data. In light of this incomplete understanding of the reaction, alternative mechanistic interpretations must be considered. These mechanistic pathways should account for the following experimental observations from this study: (i) near first-order dependence on H$_2$ pressure; (ii) O$_2$ activation through the proton-mediated generation of Au-OOH, as indicated by the O$_2$ reaction order; (iii) strong inhibition by physisorbed water on the support, which implicates the MSI as an important reaction site.

Density Functional Theory Calculations. Given the inconsistencies between the traditional homolytic H$_2$ activation model and our kinetic measurements, we performed DFT calculations to better understand the interactions between H$_2$, water, and the catalyst. To this end, we used a sophisticated model of the Au/TiO$_2$ interface in order to capture the key features of the real system. Notably, the nanorod model shown in Figure 1 exposes two distinct hydroxyl groups at the MSI: a bridge hydroxyl, bridge-OH, and a terminal (cus = coordinatively undersaturated) hydroxyl, cus-OH. These surface hydroxyls, which have different acid/base properties, are necessary to represent the experimental conditions where water is present in the system. We note that we examine the limiting case of full hydroxylation, which is equivalent to dissociatively adsorbing 1 MLE of water onto the stoichiometrically terminated rutile TiO$_2$(110) surface. The high surface hydroxyl coverage destabilizes individual OH species and increases their reactivity, but affords the advantage of eliminating artificial charge imbalances and maintains the key electronic structure features of stoichiometric TiO$_2$. The SI contains a density of states analysis showing that hydroxylation induces minimal differences in the band gap and electronic states near the Fermi level that determine chemical reactivity. These important features set this model apart from previous interface models[99−102] and are shown below to improve our ability to model interface reactivity.

The initial exposure of water to stoichiometrically terminated TiO$_2$(110) leads to the strongly exothermic

Figure 4. Hydrogen reaction order plots for P_{H_2} = 20−120 Torr (3−20 vol %). (A) Au/TiO$_2$ H$_2$ reaction orders under four different water pressures: 12 Torr H$_2$O (darkest green), 9 Torr H$_2$O (lighter), 6 Torr H$_2$O (lighter again), and 5 Torr H$_2$O (lightest). Reaction orders are reported in Table 1. (B) Au/Al$_2$O$_3$ H$_2$ reaction orders under four different water pressures: 12 Torr H$_2$O (darkest green), 9 Torr H$_2$O (lighter), 6 Torr H$_2$O (lighter again), and 5 Torr H$_2$O (lightest).

where k_2 is the rate constant for step S1-2 and k_3 is the rate constant of step S1-3. Note that the derived rate law has a maximum H$_2$ dependence of 0.5; our kinetic data show this value to be 0.64 ± 0.05 for Au/TiO$_2$ and 0.83 ± 0.08 for Au/Al$_2$O$_3$. This rate law has the associated double-reciprocal form (eq 3):

$$\frac{1}{v_{homo}} = \frac{1}{k_2[\text{Au}]_T}\left(\frac{1}{P_{H_2}^{0.5}}\right) + \frac{(1 + K'_{O_2}P_{O_2})}{k_3 K'_{O_2}P_{O_2}[\text{MSI}]_T[\text{Au}]_T} \tag{3}$$

Two kinetic parameters, v_{max} and K_R, can be extracted from eq 3 (eqs 4 and 5):

$$v_{max} = \frac{1}{\text{intercept}} = \frac{k_3 K'_{O_2}P_{O_2}[\text{Au}]_T[\text{MSI}]_T}{1 + K'_{O_2}P_{O_2}} \tag{4}$$
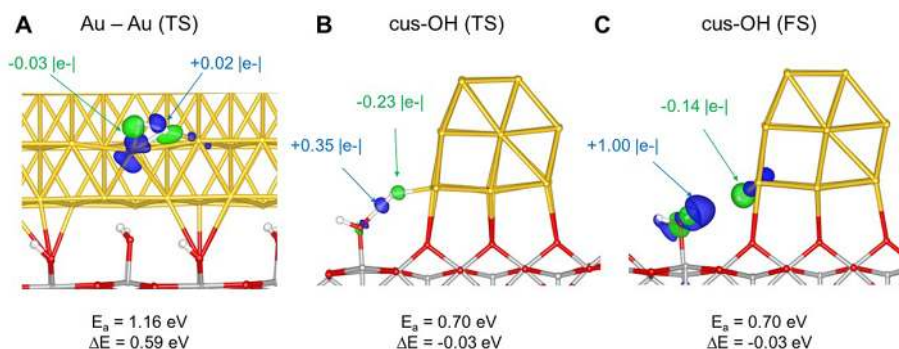
Figure 6. Charge density difference plots for H_2 dissociation calculated for (A) the transition state (TS) for homolytic H_2 dissociation on Au–Au sites away from the MSI; (B) the transition state for heterolytic H_2 dissociation on cus-OH and Au/TiO$_2$ MSI sites; (C) the final state (FS) for dissociation on cus-OH and Au/TiO$_2$ MSI sites. Green shading (negative charge) shows electron accumulation, and blue shading (positive charge) shows electron depletion.

Table 2. DFT Reaction Energies (ΔE) and Activation Energies (E_a) for H_2 Activation on Various Sites on Au/TiO$_2$

Activation Site	Mechanism	ΔE (eV)	E_a (eV)
Au-Au	Homolytic	0.59	1.16
Au$_{MSI}$-Au$_{MSI}$	Homolytic	0.79	1.27
Au$_{MSI}$-bridge-OH	Heterolytic	0.44	1.15
Au$_{MSI}$-cus-OH[a]	Heterolytic	-0.03	0.70
Au$_{MSI}$-cus-OH (dry)[b]	Heterolytic	0.21	0.91

[a]All exposed TiO$_2$ sites are hydroxylated to approximate wet conditions. [b]The TiO$_2$ support is stoichiometrically terminated (dry) except for a single pair of cus-OH and bridge-OH sites.

formation of cus-OH and bridge-OH sites ($\Delta E = -1.01$ eV/ H$_2$O). When additional water physisorbs to the hydroxylated support, it preferentially adsorbs on the bridge-OH at the Au/ TiO$_2$ interface with a binding energy of -0.53 eV/H$_2$O. In comparison, physisorption of water near the bridge-OH sites away from the interface is exothermic by -0.30 eV/H$_2$O. Water adsorption onto the Au sites (-0.19 eV/H$_2$O) is weaker still. This binding preference is consistent with earlier work using a Au$_{10}$/TiO$_2$ nanocluster model, and the generally weaker binding on Au sites for the nanorod model (relative to the Au$_{10}$/TiO$_2$ model) can be attributed to the higher Au coordination number in the nanorod model.

From the experimental H$_2$ oxidation kinetics, we can infer that the reaction is limited by hydrogen availability on the surface and that O$_2$ is not involved in H$_2$ activation. We report here two possible mechanisms for H$_2$ activation on Au/TiO$_2$. The dominant homolytic H$_2$ dissociation pathway on nanorod Au–Au sites resembling a (211) step geometry (CN = 7) away from the MSI is thermodynamically unfavorable ($\Delta E = +0.59$ eV) and is associated with a large activation barrier ($E_a = 1.16$ eV, Figure 6A). The absence of a significant support effect is corroborated in Table S1, showing that control simulations on a Au(211) slab yield nearly identical values for ΔE and E_a.

Homolytic activation of H$_2$ at Au sites near the MSI, where the edge Au atoms are also coordinated to support Ti and O atoms (CN = 6+), is even less favorable ($\Delta E = 0.79$ eV, $E_a = 1.27$ eV). Our calculated values for the activation barrier for H$_2$ dissociation at the Au sites afforded by the nanorod model agrees with the value of 1.1 eV reported for a periodic Au(111) slab,[103] but is significantly higher than the barrier of only 0.27 eV over an unsupported 12-atom cluster.[104] These values indicate that homolytic H$_2$ activation on Au sites even along the interface is expected to be slow, unless highly under-

coordinated sites are present. This interpretation is consistent with the widely reported observation that Au is a poorly active hydrogenation catalyst.

We also examined H–H bond activation across the MSI as depicted in Figure 6B and C; the reaction energies and associated activation barriers are summarized in Table 2. H$_2$ adsorption at the MSI is essentially thermoneutral ($\Delta E = -0.03$ eV), and the associated activation barrier ($E_a = 0.70$ eV) is almost half that of the barrier at Au step sites on the nanorod ($E_a = 1.16$ eV). Figure 6B also shows that H$_2$ activation at the MSI proceeds through more complicated interactions with both the metal and support cus-OH sites, resulting in heterolytic H–H bond cleavage, with a proton residing on the support hydroxyl and a formal hydride on the Au. We note that heterolytic H$_2$ dissociation involving a bridge-OH site (which has weak Brønsted acid character) has a moderate thermodynamic barrier ($\Delta E = 0.44$ eV) and a correspondingly higher activation barrier ($E_a = 1.15$ eV). Both of these values are comparable to the homolytic cleavage at (211)-type Au sites away from the MSI. Further, we note that H$_2$ activation on cus-OH is affected by hydroxyl stability, and the saturation of the TiO$_2$ surface with dissociated water increases the cus-OH reactivity. These effects are quantified in the SI and limit the maximum barrier for heterolytic H$_2$ activation on cus-OH to $E_a = 0.91$ eV across the MSI when the TiO$_2$ surface is incompletely hydroxylated.

Given the high pK_a value for H$_2$ (36),[105] the DFT prediction of a heterolytic H–H cleavage pathway is surprising, so we sought further insight into the potential driving forces for this reaction pathway. We examined the electron density redistribution for both heterolytic and homolytic H$_2$ activation using Bader charge analysis. H$_2$ adsorption on top of the nanorod shows symmetric charge density distribution and

equal Bader charges for each H atom in the transition state (Figure 6A). This traditional homolytic H_2 adsorption pathway also shows little electron transfer from Au to the (formal) dihydrides. Gold is one of the few metals more electronegative than hydrogen, so the highly covalent nature of the Au−H bonding is not surprising; further, the difficulty of formally oxidizing Au is consistent with the thermodynamic unfavorability of this step.

The atomic charges from the Bader analysis are referenced to the initial states of H_2 dissociation. The transition state Bader analysis of the heterolytic MSI pathway (Figure 6B) shows a relatively early transition state with a +0.35 |e⁻| charge on the developing proton. The developing hydride, however, has a slightly smaller negative charge, indicating that some of the negative charge is transferred to the Au nanorod. This is confirmed by the Bader analysis of the final state (Figure 6C), which shows −0.14 |e⁻| charge on the (formal) hydride, −0.11 |e⁻| charges distributed across the Au nanorod, a charge of −0.50 |e⁻| transferred to the oxygen in the cus-OH site, −0.14 |e⁻| charges distributed on Ti atoms, and the balance of −0.11 |e⁻| charges distributed over the remaining oxygen atoms.[106] The H_2 dissociation involving the bridge-OH site is also heterolytic in nature with a similar charge of +0.38 |e⁻| on the developing proton in the transition state.

Infrared Spectroscopy. If the heterolytic H_2 adsorption pathway predicted by the DFT studies is correct, we should expect to see rapid exchange between gas phase hydrogen and support protons. To test this hypothesis, we used infrared spectroscopy to monitor H_2 adsorption on a D_2O-exchanged Au/TiO_2 catalyst. Figure 7 shows the evolution of the O−H(D) region of the IR spectrum over time after the introduction of H_2; the D_2O exchanged catalyst was collected as a background spectrum to more easily observe the changes upon H_2 adsorption. The growth of the broad band at ∼3300 cm⁻¹ (ν_{O-H}) is consistent with the rapid addition of H-bonded protons upon introducing H_2 to the catalyst. The loss of the band at 2700 cm⁻¹, which is associated with non-H-bonded or "dangling" −OD bands similarly indicates that these −OD groups become involved in H-bonding interactions when H_2 is added to the system. The increase of the band at ∼1600 cm⁻¹ (δ_{H-O-H}) and 1400 cm⁻¹ (δ_{D-O-H}) and the loss of the band at 1200 cm⁻¹ (δ_{D-O-D}) is also consistent with proton exchange between H_2 and the deuterated support.

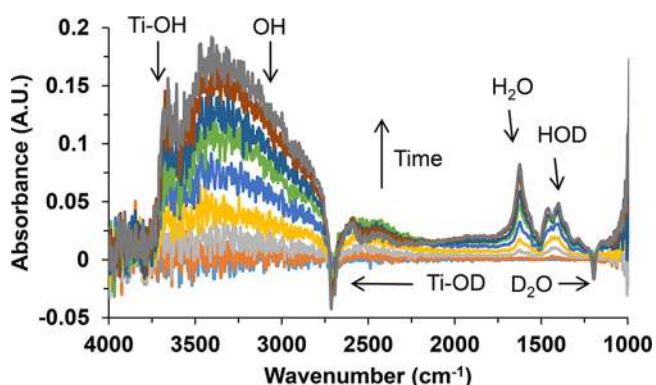**Figure 7.** FTIR spectra of H_2 adsorption on a D_2O-exchanged Au/TiO_2 catalyst. T = 70 °C, H_2 WHSV = 40 L/g_{cat}/h. The data, collected over 30 min, show the evolution of O−H bands attributable to H−D exchange during H_2 adsorption.

Heterolytic H_2 adsorption at the MSI sites requires the H−D exchange, so the observed changes in Figure 7 are consistent with this mechanism. Further, they exclude the possibility that H_2 adsorption occurs exclusively on the metal; if this were the case, no exchange with the support would be observed. The results in Figure 7 are also consistent with homolytic adsorption followed by fast exchange with the support. As discussed below, this is kinetically indistinguishable from heterolytic adsorption, although the DFT calculations suggest that heterolytic activation is the more likely pathway. Additionally, by using the molar absorptivity for weakly adsorbed water for FTIR,[13] a rate for water formation can be extracted from Figure 7. This rate represents a lower limit for H_2 activation, considering this is not a direct measure of the activation itself. Rather, it measures the rate of water formation, which requires the formation of two O−H bonds on a single O atom and is an approach to the equilibrium distribution of all protons and deuterons in the system. The rate extracted from Figure 7 was 0.0113 ± 0.0001 mol$_{H_2O}$/mol$_{Au}$/s, which is generally consistent with the rates measured for H_2 oxidation.

Hydrogen Spillover and Metal−Support Proton Exchange. The terms used to describe hydrogen spillover and proton exchange processes (generally revealed through H−D exchange experiments) are often used interchangeably in the literature. To clearly define these processes, we refer to Prins' discussion in a recent review.[107] The term "spillover" was originally coined by Boudart and Vannice to describe the migration of H atoms from the metal particles to the support, because the H atoms spill over, as it were, from a hydrogen-rich to a hydrogen-poor surface.[107] The term is typically applied to metals that adsorb hydrogen strongly (e.g., Pt, Rh) and is most commonly employed to describe processes that occur at elevated temperatures. Given the weak binding of H_2 to Au[98,108] and the low H surface coverages accessible under these H_2 pressures, it is difficult to describe Au as a hydrogen-rich surface. The term "hydrogen spillover", at least as it is classically defined, probably is not an appropriate description of the chemistry we observe. Prins also points out that Brønsted acid−base chemistry can induce H−D exchange on nonreducible supports and highlights examples where H−D exchange is observed but not attributable to hydrogen spillover.[109,110]

On reducible supports, hydrogen spillover may be better described as a proton-coupled electron transfer in which the proton transfers to the metal oxide surface and an electron through the metal cations. For Au/TiO_2, there are intimate electronic interactions between the metal and the support, and adsorbing CO appears to induce a partial reduction of the underlying support.[111] While we believe that the bulk of evidence better supports heterolytic activation at the MSI, it is also consistent with homolytic activation followed by fast deprotonation by the support. Under this description, the H−D exchange that we observe could also be considered as hydrogen spillover. Presumably these processes are at work in the all-proton systems as well.

We also examined the possibility that the observed reaction kinetics and H−D exchange might be due to homolytic H_2 activation followed by fast deprotonation by the support. The potential energy diagram for this pathway is graphed in red in Figure 8 and juxtaposed against the direct heterolytic activation pathway in blue. We note that the energy values
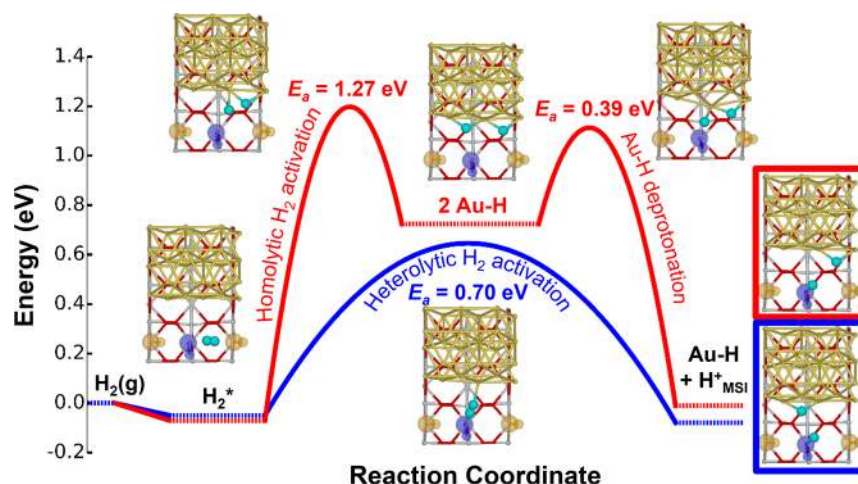
Figure 8. Potential energy diagram comparing the heterolytic H_2 activation across the MSI at a cus-OH site (blue) with homolytic H_2 activation on Au_{MSI} followed by deprotonation (red). $H_2(g)$ is used as reference energy.
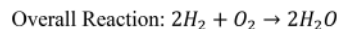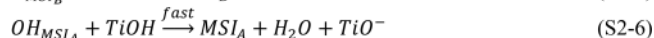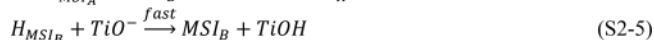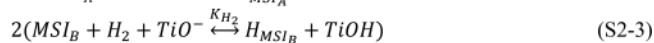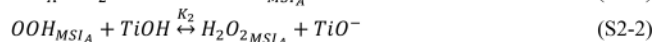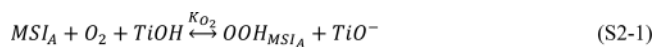
used in Figure 8 are strictly for the MSI. Homolytic H_2 activation sites with slightly more favorable energetics exist away from the interface as discussed earlier and shown in Table 2; however, these sites are incapable of undergoing proton transfer to the support. It is not surprising that the final states for direct heterolytic adsorption and homolytic adsorption followed by deprotonation are essentially equivalent both structurally and energetically (Table 2).

Both the potential energy diagram in Figure 8 and the activation energetics summarized in Table 2 are consistent with heterolytic dissociation across the interface as the dominant H_2 activation route with a significantly lower barrier to final states that differ only in the location of the Au−H (Figure 8, Table S3). The exothermic nature of the proton transfer step suggests that the formal oxidation of Au during homolytic cleavage makes this process unfavorable. It also indicates that heterolytic cleavage is the preferred pathway because it avoids this formal oxidation. It is also noteworthy that deprotonation of the formal Au hydride by the support is energetically favorable and has only a moderate kinetic barrier of 0.39 eV. This is consistent with the electronegativity of Au providing the driving force for deprotonation. Importantly, this facile deprotonation could result in transfer of all the hydrogens to the support via deprotonation pathways regardless of whether they resulted from homolytic or heterolytic cleavage.

Heterolytic H_2 Activation Kinetic Model. Since the DFT and FTIR studies suggest heterolytic H_2 activation at the MSI as the likely pathway, the H_2 dependence data in Figure 4 was re-evaluated using a kinetic model consistent with this mechanism. This pathway also allows us to carefully consider the involvement of support protons (and therefore acid−base centers) in the reaction mechanism. The DFT calculations suggest that H_2 activation occurs at MSI sites with access to basic hydroxyls, and O_2 activation at MSI sites requires acidic hydroxyls (or water). We therefore distinguish between H_2 and O_2 activation sites with the following nomenclature: O_2 activation occurs at MSI_A and H_2 activation occurs at MSI_B (A = acidic, B = basic).

We first examine the possibility that the reaction is hydrogen coverage limited. If H_2 activation was the only important kinetic step, one would expect the kinetics to be first order in hydrogen and zeroth order in oxygen. While the experimental

Scheme 2. Elementary Steps for H_2 Oxidation via Heterolytic H_2 Activation on Au[a]

$$MSI_A + O_2 + TiOH \overset{K_{O_2}}{\longleftrightarrow} OOH_{MSI_A} + TiO^- \qquad (S2\text{-}1)$$

$$OOH_{MSI_A} + TiOH \overset{K_2}{\longleftrightarrow} H_2O_{2_{MSI_A}} + TiO^- \qquad (S2\text{-}2)$$

$$2(MSI_B + H_2 + TiO^- \overset{K_{H_2}}{\longleftrightarrow} H_{MSI_B} + TiOH) \qquad (S2\text{-}3)$$

$$H_2O_{2_{MSI_A}} + H_{MSI_B} \overset{k_4}{\longrightarrow} MSI_B + OH_{MSI_A} + H_2O \qquad (S2\text{-}4)$$

$$H_{MSI_B} + TiO^- \overset{fast}{\longrightarrow} MSI_B + TiOH \qquad (S2\text{-}5)$$

$$OH_{MSI_A} + TiOH \overset{fast}{\longrightarrow} MSI_A + H_2O + TiO^- \qquad (S2\text{-}6)$$

Overall Reaction: $2H_2 + O_2 \rightarrow 2H_2O$

[a]MSI_A sites are Au sites directly at the MSI with access to an acidic hydroxyl; MSI_B sites have access to a basic hydroxyl. The r.d.s. is considered to be the reaction between $H_2O_{2_{MSIA}}$ and H_{MSI_B} (step S2-4).

reaction orders are consistent with the rate law describing this mechanism (details in the SI), if the reaction was truly limited by heterolytic H_2 activation, one would expect the measured kinetics to be closer to unity. It appears more likely that the reaction is limited by H coverage, i.e., that a high H_2 activation barrier leads to sufficiently low H coverage to limit the rate of a subsequent step with a lower activation barrier. The most likely candidate for this limiting step is a slow reaction between Au−H and activated O_2 (see additional DFT calculations below). Scheme 2 presents this mechanism, assuming that H_2 adsorption is quasi-equilibrated (step S2-3 can therefore be described with K_{H_2}) and that the reaction between the formal Au hydride and adsorbed H_2O_2 is rate determining.

Initially ignoring the effects of water, a Langmuir−Hinshelwood treatment of the MSI_B sites yields the rate law in eq 6 under constant H_2O pressure (details in the SI).

$$\nu_{hetero} = \frac{k_4 K_2' K_{H_2}' P_{H_2} K_{O_2}' P_{O_2} [MSI_A]_T [MSI_B]_T}{(1 + K_{H_2}' P_{H_2})(1 + K_{O_2}' P_{O_2} + K_2' K_{O_2}' P_{O_2})} \qquad (6)$$

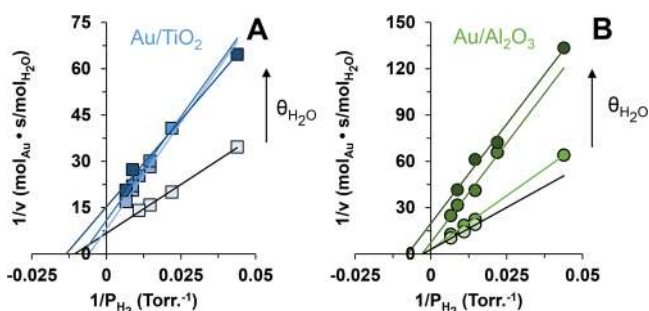The associated double-inverse form of the rate law is presented in eq 7:

Figure 9. Lineweaver–Burk plots for H_2 oxidation catalysis at 60 °C under several different water pressures. (A) Au/TiO$_2$ data under the following P_{H2O} values: 12 Torr (darkest), 9 Torr (lighter), 6 Torr (lighter again), and 5 Torr (lightest). (B) Au/Al$_2$O$_3$ data under the following P_{H2O} values: 12 Torr (darkest), 9 Torr (lighter), 6 Torr (lighter again), and 5 Torr (lightest). Reactions were carried out at 60 °C with 10 vol % O$_2$, 3–20 vol % H$_2$, 5–12 Torr H$_2$O, at WHSV = 2.3×10^3 L/g$_{cat}$/h. The extracted Michaelis–Menten parameters are reported in Table 3.

$$\frac{1}{v_{hetero}} = \frac{1}{k_{obs}K'_{H_2}[MSI_A]_T[MSI_B]_T}\left(\frac{1}{P_{H_2}}\right) + \frac{1}{k_{obs}[MSI_A]_T[MSI_B]_T} \quad (7)$$

where k_{obs} is the combined rate constant defined in eq 8:

$$k_{obs} = \frac{k_4 K'_2 K'_{O_2} P_{O_2}}{(1 + K'_{O_2}P_{O_2} + K'_2 K'_{O_2}P_{O_2})} \quad (8)$$

The v_{max} and K_R kinetic parameters can be defined and extracted using eqs 9 and 10:

$$v_{max} = \frac{1}{intercept} = k_{obs}[MSI_A]_T[MSI_B]_T \quad (9)$$

$$K_R = \frac{slope}{intercept} = \frac{1}{K'_{H_2}} \quad (10)$$

This mechanism is readily evaluated with double-reciprocal (Lineweaver–Burk) plots; Figure 9 shows this treatment does a far better job of describing the H$_2$ dependence data than does the homolytic H$_2$ activation mechanism (Figure 5). For both
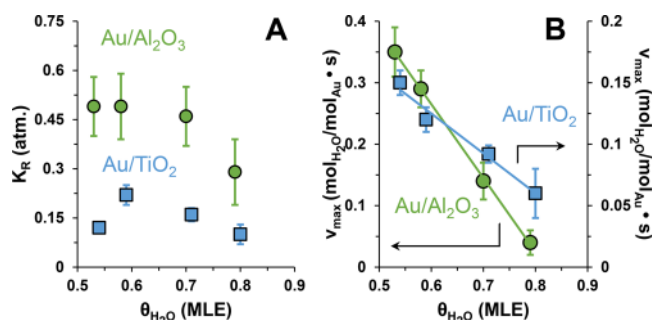
Figure 10. Extracted H$_2$ oxidation kinetics parameters as a function of weakly adsorbed water coverage in Langmuir monolayer equivalents (MLE). (A) K_R vs θ_{H_2O} for Au/TiO$_2$ (blue squares) and Au/Al$_2$O$_3$ (green circles). (B) v_{max} vs θ_{H_2O} for Au/TiO$_2$ (blue squares) and Au/Al$_2$O$_3$ (green circles). Reaction conditions: 60 °C, 10 vol % O$_2$, 3–20 vol % H$_2$, 5–12 Torr H$_2$O, at WHSV = 2.3×10^3 L/g$_{cat}$/h.

catalysts, v_{max} terms vary linearly with the feedwater content, while the K_R terms show relatively little change. This is essentially "noncompetitive inhibition" in the Michaelis–Menten terminology. The extracted descriptive parameters (K_R and v_{max}, Figure 10 and Table 3) show that water has essentially no effect on the H$_2$ binding equilibrium (K_R), while v_{max} is inversely related to weakly adsorbed water coverage. It is unlikely that the net rate constant (k_{obs}) varies linearly with water pressure, so the most reasonable conclusion is that the number of available active sites ($[MSI_B]_T$) decreases as water is added to the system. This behavior is consistent with water physically blocking the H$_2$ activation sites, as we have observed in other reactions with other reaction poisons.[93,94]

The water poisoning can be added to the simplified rate law with the simple assumption that the physisorbed water binds to the support, but not preferentially at the MSI. Thus, Au$_{MSI}$ site availability is proportional to the fraction of the oxide surface that is not covered by water and inversely proportional to the weakly adsorbed water coverage on the support (eq 12, more details in the SI). Additionally, CO oxidation, which may report on O$_2$ activation, shows a similar inverse first-order dependence on water at these water pressures (data in the SI). Thus, the addition of a simple water site blocking term is consistent with the loss of both H$_2$ and O$_2$ activation sites. Equations 12 and 13 show the heterolytic rate law and

**Table 3. Michaelis–Menten Parameters Extracted from Figure 9 for H$_2$ Oxidation**[a]

Catalyst	P_{H2O} (Torr.)	θ_{H2O}	K_R (atm)	K_{H_2} (atm^{-1})	v_{max} (s^{-1})
Au/Al$_2$O$_3$	12	0.79	0.29 ± 0.09	3.4 ± 1.1	0.04 ± 0.02
	9	0.70	0.46 ± 0.09	2.2 ± 0.4	0.14 ± 0.03
	6	0.58	0.5 ± 0.1	2.0 ± 0.4	0.27 ± 0.03
	5	0.53	0.49 ± 0.07	2.0 ± 0.3	0.35 ± 0.04
	Average		0.44 ± 0.09	2.4 ± 0.6	---
Au/TiO$_2$	12	0.80	0.09 ± 0.03	11.1 ± 3.7	0.06 ± 0.02
	9	0.72	0.16 ± 0.02	6.3 ± 0.8	0.092 ± 0.007
	6	0.59	0.22 ± 0.03	4.6 ± 0.6	0.12 ± 0.01
	5	0.54	0.13 ± 0.01	7.7 ± 0.6	0.15 ± 0.01
	Average		0.15 ± 0.02	7.4 ± 2.4	---

[a]Reaction conditions: 60 °C, 10 vol % O$_2$, 3–20 vol % H$_2$, 5–12 Torr H$_2$O, WHSV = 2.3×10^3 L/g$_{cat}$/h.

Table 4. DFT Results Describing Elementary Steps, with Associated Reaction Energies (ΔE) and Activation Barriers (E_a), for the Metal-Only and Proton-Enabled Reaction Pathways during H_2 Oxidation. Protons on the Support Near the MSI are Denoted H^+_{MSI} and Compensating e^- Charges are Assumed to be Distributed across the Metal and the Support.

		Metal-only Elementary Steps		
Entry	**Step**	**Reaction**	**E_a (eV)**	**ΔE (eV)**
M1	H_2 activation (homolytic)	$2Au + H_2 \rightarrow 2Au\text{-}H$	1.16	0.59
M2	OOH dissociation	$Au\text{-}OOH + Au \rightarrow Au\text{-}O + Au\text{-}OH$	0.99	-0.34
M3	H_2O_2 formation	$Au\text{-}OOH + Au\text{-}H \rightarrow Au\text{-}H_2O_2 + Au$	0.59	-1.23
M4	H_2O_2 reaction with Au-H	$Au\text{-}H_2O_2 + Au\text{-}H \rightarrow Au\text{-}OH + Au\text{-}H_2O$	0.31	-2.77
M5	H_2O_2 dissociation	$Au\text{-}H_2O_2 + Au \rightarrow 2Au\text{-}OH$	0.55	-0.82
M6	OH reaction with Au-H	$Au\text{-}OH + Au\text{-}H \rightarrow Au\text{-}H_2O + Au$	0.61	-1.59
M7	OH disproportionation	$2Au\text{-}OH \rightarrow Au\text{-}O + Au\text{-}H_2O$	0.41	-0.33
M8	Au-O reaction with Au-H	$Au\text{-}O + Au\text{-}H \rightarrow Au\text{-}OH + Au$	1.01	-1.74
		Proton Enabled Elementary Steps at the Metal-Support Interface		
Entry	**Step**	**Reaction**	**E_a (eV)**	**ΔE (eV)**
P1	H^+ exchange on support	$cus\text{-}OH_2^+ + br\text{-}0^- \rightarrow cus\text{-}OH + br\text{-}OH$	0.49	0.08
P2	Au-H deprotonation	$Au\text{-}H \rightarrow Au + H^+_{MSI}$	0.39	-0.73
P3	O_2 activation	$Au + O_2 + H^+_{MSI} \rightarrow Au\text{-}OOH$	0.05	-0.49
P4	H_2 activation (heterolytic)	$Au + H_2 \rightarrow Au\text{-}H + H^+_{MSI}$	0.70	-0.03
P5	Au-OOH protonation	$Au\text{-}OOH + H^+_{MSI} \rightarrow Au\text{-}H_2O_2$	0.04	-0.27
P6	H_2O_2 protonation	$Au\text{-}H_2O_2 + Au + H^+_{MSI} \rightarrow Au\text{-}OH + Au\text{-}H_2O$	0.41	-1.81
P7	Au-OH protonation	$Au\text{-}OH + H^+_{MSI} \rightarrow Au\text{-}H_2O$	0.00	-1.17
P8	Au-O protonation	$Au\text{-}O + H^+_{MSI} \rightarrow Au\text{-}OH$	0.16	-1.04

associated double-inverse equation, respectively, with water site blocking included:

$$MSI + H_2O \xleftrightarrow{K_{H_2O}} MSI(H_2O) \tag{11}$$
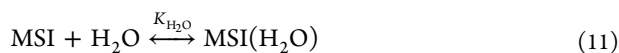
$$\nu_{hetero} = \frac{k_4 K'_2 K'_{H_2} P_{H_2} K'_{O_2} P_{O_2} [MSI_A]_T [MSI_B]_T}{(1 + K'_{H_2} P_{H_2})(1 + K'_{O_2} P_{O_2} + K'_2 K'_{O_2} P_{O_2})(1 + K_{H_2O} P_{H_2O})} \tag{12}$$

$$\frac{1}{\nu_{hetero}} = \frac{(1 + K_{H_2O} P_{H_2O})}{k_{obs} [MSI_A]_T [MSI_B]_T K'_{H_2}} \left(\frac{1}{P_{H_2}} \right) + \frac{(1 + K_{H_2O} P_{H_2O})}{k_{obs} [MSI_A]_T [MSI_B]_T} \tag{13}$$

$$\nu_{max} = \frac{1}{intercept} = \frac{k_{obs} [MSI_A]_T [MSI_B]_T}{1 + K_{H_2O} P_{H_2O}} \tag{14}$$

$$K_R = \frac{slope}{intercept} = \frac{1}{K'_{H_2}} \tag{15}$$

New descriptive parameters, which include the water site blocking term, can also be defined (eqs 14 and 15). These

parameters agree with the experimental data showing that ν_{max} decreases and K_R remains constant as water coverage increases.

The mechanism shown in Scheme 2 and the associated rate law (eq 12) are broadly consistent with the kinetic data. The kinetic plots also provide several independent measures of the H_2 adsorption equilibrium constant (K_{H_2}). These values (2.4 ± 0.6 atm^{-1} for Au/Al$_2$O$_3$ and 7 ± 2 atm^{-1} for Au/TiO$_2$) are reasonably small and appropriately describe the weak binding of H_2 to Au catalysts. These values are entirely in line with the near-thermoneutral H_2 binding predicted by the DFT model. Since the kinetics for the two systems are essentially the same, we postulate that they proceed through similar mechanisms. It is likely that the general nature of the proton-assisted pathways is similar on Au/Al$_2$O$_3$ catalysts, although we expect some differences in the ability of the nonreducible support to assist in stabilizing the negative charges associated with the Au hydride. Considering the significant computational cost, we deemed a full DFT investigation of the Au/Al$_2$O$_3$ catalyst too expensive to pursue.

There are relatively few quantitative measures of H_2 adsorption thermodynamics on supported Au catalysts, making direct comparisons with the literature difficult. Van Bokhoven and co-workers measured volumetric H_2 chemisorption over several Au/Al$_2$O$_3$ catalysts.[112] Their H:Au ratios attributable to strong chemisorption were small, varying between 5% and 20%
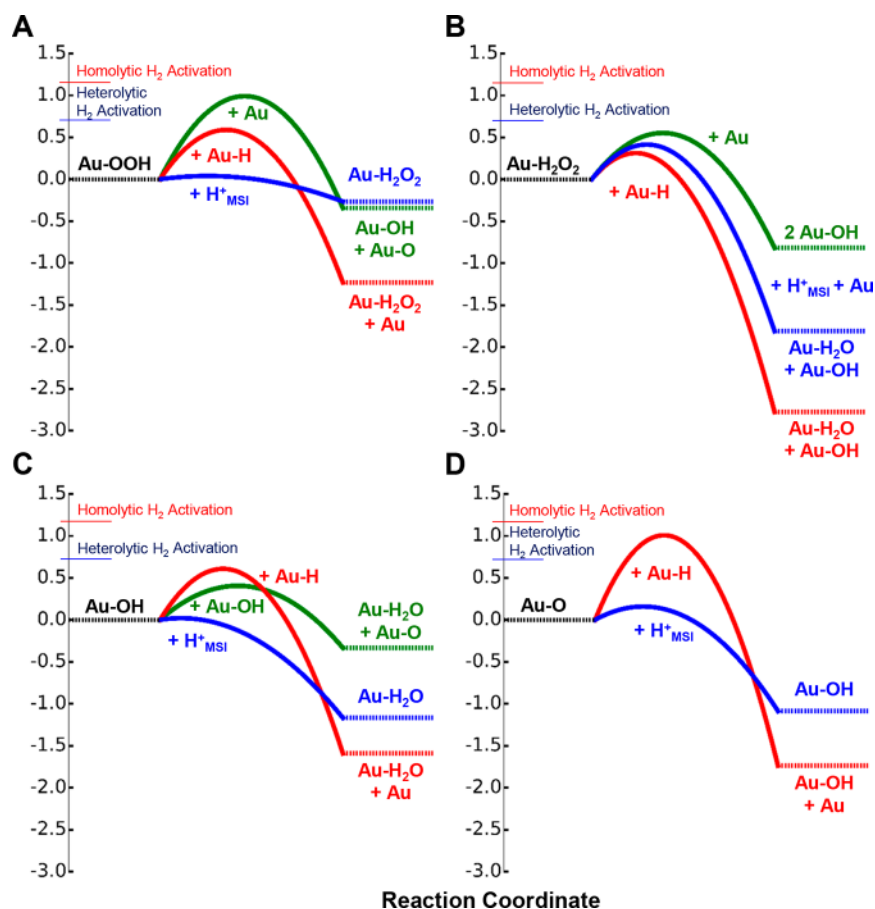
Figure 11. Reaction pathways for (A) Au-OOH, (B) Au-H_2O_2, (C) Au-OH, and (D) Au-O. The energetics, referenced to the initial state of each pathway, are set to 0 eV. Reaction with a proton from the support is designated as H^+_{MSI}; the respective pathways are shown in blue. Reactions with a formal Au hydride are designated as Au-H; the respective pathways are shown in red. All other pathways are shown in green. The blue and red extended tick marks indicate the required activation energy for heterolytic and homolytic H_2 activation, respectively.

for different catalysts over a wide range of temperatures. These values are consistent with H_2 activation at the MSI. Thomson also calculated the H_2 heat of adsorption on a series of Au/TS-1 type catalysts and found exceedingly weak heat of adsorption values around 1−2 kcal/mol.[113]

There are a few additional experimental measurements of H_2 adsorption on Au model systems. Stobinski and co-workers have reported several studies of H_2 adsorption on Au films, determining a heat of adsorption of 21 kJ/mol.[114] The weak H_2 binding sites were attributed to undercoordinated atoms at edges, corners, and kink/step sites.[115] Madix and Campbell reported very weak H_2 adsorption on hot Au filaments at low temperatures (216 K), with a dissociative activation barrier of 51 kJ/mol.[116] Note that adsorption on these Au surfaces was assumed to be traditional homolytic chemisorption, so the determined values may not be directly comparable to the heterolytic process that our data suggest. Rather, they suggest that traditional chemisorption on Au may be so weak that alternative H_2 activation pathways become more attractive explanations for the observed reactivity.

Alternative Reaction Pathways. We also considered the possibility that the reaction proceeds through a traditional homolytic cleavage mechanism away from the MSI. Dumesic's work on H_2 oxidation over supported Pt catalysts showed that H_2 chemisorption followed by a rate-determining reaction with an active oxygen species can have a maximum H_2 reaction order of 0.5. However, if a subsequent step involving Au-H is

rate determining, the observed reaction order could approach unity (derivations available in the SI). While we cannot rule such a mechanism out entirely, it is not supported by the kinetic data or the DFT calculations. Because water does not bind to Au, it is difficult to rationalize the strong water inhibition at support θ_{H_2O} values around 0.5 if the reaction does not occur at the metal−support interface. Additionally, if a later step was rate determining, we would expect a relatively high coverage of Au-OOH, since this species binds both rapidly and strongly.[13] Given the very few reports characterizing the nature of O_2 binding to Au catalysts,[117] this seems unlikely. Finally, the rapid H−D exchange demonstrated with FTIR shows that gas phase H_2 exchanges with support protons and that this rate is comparable to the overall reaction rate.

It is far more plausible that the reaction is limited by the thermodynamics and kinetics of hydrogen binding. We therefore examined the subsequent elementary steps with the DFT nanorod model; details are provided in Table S3. Table 4 compiles these results, first examining the elementary steps that occur on metal sites (i.e., without the aid of MSI protons). Note that all of the steps after homolytic H_2 activation have lower activation barriers than dissociative chemisorption. This further supports the kinetic evidence that H_2 oxidation does not proceed through this traditional pathway on Au.

The second half of Table 4 adds the elementary steps that involve proton transfer chemistry. Entry P1 shows the exchange reaction between cus-OH_2^+ and bridge-O^- is

essentially thermoneutral. Consequently, the cus-OH_2^+ and bridge-OH protons have similar acidities, and cus-OH and bridge-O^- are of similar basicity; this simplifies the surface chemistry substantially. For convenience, we consider the support as a proton source/sink and generally refer to support protons as H^+_{MSI} for the remainder of this discussion: the energetics of the processes will not change significantly if an appropriate cus-OH or bridge-OH site is used. This also helps consider the reaction kinetics: particularly in the presence of water, the support can rapidly supply protons to or remove them from species adsorbed on the metal.

Next, Au-H deprotonation by the support is thermodynamically favorable and has a lower barrier (0.39 eV) than all but one of the calculated barriers for the metal-only reactions. This suggests that even if a dissociative chemisorption mechanism was at work, deprotonation would likely be fast relative to other steps that might occur on the Au. Thus, regardless of the details of H_2 activation, the catalysis likely proceeds through the significantly faster proton-mediated chemistries that the support affords.

We evaluate the remaining possible reactions in a stepwise fashion considering each of the likely O-containing intermediates individually. Each intermediate has three nominal reaction pathways, shown graphically in Figure 11: (i) reaction with Au-H, (ii) reaction with a MSI proton (H^+_{MSI}), or (iii) reaction with a free Au site (this leads to dissociation or disproportionation depending on the nature of the intermediate). For Au-OOH (Figure 11A), Au-OH (Figure 11C), and Au-O (Figure 11D), protonation reactions are nearly barrierless and are always considerably faster than reaction with Au-H or any of the alternate pathways. The exception to this is Au-H_2O_2 (Figure 11B), which has low barriers to react with either Au-H or H^+_{MSI}. Direct dissociation of Au-H_2O_2 is also a viable reaction pathway.

These results are illuminating and highlight the special reactivity of Au catalysts. First, the relatively fast proton transfer steps enable a variety of chemistries (e.g., heterolytic H_2 activation, fast Au-OH decomposition) that are unavailable when only metal-catalyzed pathways are considered. These weak Brønsted acid–base chemistries generally have lower activation barriers than the comparable metal-only pathways. Indeed, the pathways involving H^+_{MSI} and Au-OOH, Au-OH, and Au-O are essentially barrierless despite the fact that the deprotonation energetics in Figure 8 indicate the H^+_{MSI} species to be ca. −0.7 eV more stable than Au-H. This is an intriguing result, as it indicates that the addition of weak Brønsted acid–base chemistry to the metal system breaks the predicted transition state scaling relations that hold for many other systems.[103,118−120] Readers are directed to a recent perspective by Kumar et al. for an excellent review on how interfacial sites can employ different chemistries to overcome the limitations of metal scaling relations.[121]

Second, the unfavorable energetics for formal metal oxidation, along with the associated high activation barriers, are a key feature of the Au chemistry (e.g., dissociative chemisorption/oxidative addition). Consequently, pathways that deliver electrons to the electronegative Au or avoid formal oxidation are generally more facile. Finally, the metal–support interface provides an interesting means of considering H_2 oxidation over these materials. Essentially, the fastest pathways involve supplying electrons to the Au (and ultimately to the adsorbed O species) through H_2 adsorption. Protons are concurrently delivered to the support via heterolytic H_2

adsorption and Au−H deprotonation. These Au catalysts function essentially via proton-coupled electron transfer mechanisms, with hydrogen electron density distributed both to the Au atoms and, at least for titania, the underlying support. In a sense, this mechanism can be considered as being closely related to electrochemical reactions, with (conceptually) hydrogen activation and deprotonation occurring at basic MSI sites and O_2 activation occurring at acidic MSI sites. The Au (with help from the support) then serves as electron source/sink, depending on the half-reaction. This is shown conceptually in Scheme 3.

Scheme 3. Graphic Representation of H_2 Oxidation over Supported Au Catalysts
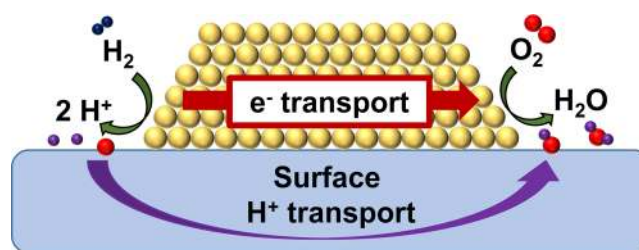
These processes are remarkably similar to those that Wilson and Flaherty have identified in their detailed examination of the liquid phase partial reduction of O_2 to H_2O_2 over Pd/SiO_2 and PdAu/SiO_2 catalysts.[122,123] Their work showed that protic solvents, which act as fast proton carriers whose concentration is determined by solution pH, dramatically improve catalyst activity. In our work protons are transferred across the hydroxylated and/or water-covered support; their chemical potential is determined by the pressures of H_2O and H_2. One of the key differences between the two systems is that O_2 activation on Au requires a proton to generate Au-OOH in a single step, while the Pd system appears to go through a series of stepwise proton−electron transfer steps mediated by a protic solvent. The considerably less favorable and site-specific activation of H_2 at the MSI for Au catalysts is also an important difference in these systems. These observations are consistent with the support effects Hutchings and co-workers observe in their PdAu H_2O_2 synthesis catalysts after acid pretreatments.[124−126]

Implications for PrOx. Our initial motivation for studying H_2 activation was to better understand the role of water in improving the PrOx reaction. It is now clear that water plays two beneficial roles during PrOx. First, water, or another proton source, is required for fast CO oxidation, as it is involved in both O_2 activation and rate-determining Au-COOH decomposition.[13] Second, water clearly poisons H_2 activation at the MSI. This suggests that a less volatile proton source at the MSI can accomplish two complementary goals: (i) it may be possible to suppress H_2 activation by selectively blocking the MSI sites without poisoning the desirable CO oxidation reaction, and (ii) faster CO oxidation rates may be achieved at higher temperatures at which physisorbed water would readily desorb. Either of these outcomes would constitute a significant improvement to the process conditions for the PrOx reaction.

Comparisons to Other H_2 Activation Systems. There are numerous precedents for heterolytic H_2 activation mechanisms in the enzyme and inorganic chemistry literature. Several groups have suggested heterolytic H_2 activation by

hydrogenases,[127−131] and Crabtree has shown that Ni−Fe hydrogenases employ a heterolytic H_2 activation process, resulting in a formal hydride on the (unoxidized) Ni and a proton on an adjacent bridging oxo group. This conclusion has been supported by DFT calculations and substantial synthetic modeling and is fundamentally similar to what we observe for the Au catalysts. Several systems of transition metal complexes have been shown to activate H_2 heterolytically.[132−141] Metal hydrides have long been known to be acidic,[142,143] so these systems might be considered as operating via the traditional oxidative addition mechanism followed by rapid deprotonation. There is also now a fairly extensive literature of heterolytic H_2 dissociation using frustrated Lewis pairs (FLPs), which can be used to perform a variety of organic hydrogenations without the use of transition metals.[50−52] Heterolytic H_2 activation has also been implicated at the Ru/TiO_2 MSI during hydrodeoxygenation of phenols. In this case, the heterolytic activation step was suggested as an alternative to hydrogen spillover to the titania support; the homolytic dissociation of H_2 over ruthenium metal sites remains the fastest H_2 scission pathway in this system.[144,145]

The dominant heterolytic H_2 activation over a supported metal catalyst is a surprising discovery; we are aware of exceedingly few examples of solid systems that have reported convincing experimental evidence of this general pathway. Notably, Copéret and co-workers have shown that γ-Al_2O_3, when treated at appropriately high temperatures, can activate H_2 and catalyze the hydrogenation of simple alkenes. The thermal treatment generates defect sites on the alumina surface, which effectively function as FLPs. Tomishige and co-workers also found a first-order hydrogen dependence in studying hydroxyl-containing ether hydrogenolysis over Re-modified supported Rh catalysts.[146] They similarly argued that the hydrogen dependence was most consistent with a net heterolytic activation of H_2, with the proton being transferred to the water solvent and the hydride being stabilized by the Rh. Further, Stair and co-workers have also recently prepared single-site supported aluminum catalysts on catechol-containing porous organic polymers.[147] These materials hydrogenate alkenes through H_2 insertion into Al−O bonds, resulting in a formal hydride on the aluminum atom.

Several groups have shown that the addition of Brønsted bases increases the hydrogenation activity of supported Au catalysts. For example, Cao and co-workers reported that the addition of quinolines dramatically improved hydrogenation activity over Au while suppressing activity over Pt, Pd, and Ru catalysts.[148] The addition of a variety of amine bases, including cycloaliphatic diamines, to several supported Au catalysts resulted in improved alkyne partial hydrogenation activity. In their study, Rossi and co-workers considered these Au-amine systems to be FLPs.[149,150] Similar improvements in 1,3-cyclohexadiene partial hydrogenation were found for Au particles suspended in imidazolium ionic liquids.[151] In all these studies, heterolytic H−H bond activation was implicated in the improved activity. We also note that incorporating secondary phosphine oxide ligands into solution-phase ligand stabilized Au nanoparticles (NPs) resulted in improved activity and selectivity in cinnamaldehyde hydrogenation. These clever systems incorporated a basic oxo group into the phosphine to assist in heterolytic H_2 activation.[152,153]

The heterolytic activation of H_2 over Au catalysts therefore has significant precedent in other similar chemistries. This literature also provides some important context to understand this system. The active sites at the MSI can be considered to be composed of a Brønsted base (surface hydroxyl), which stabilizes the developing proton in close proximity to a soft Lewis acid[154] (Au NP), which stabilizes the developing hydride. The surface hydroxyls on alumina and titania are not particularly strong bases, which suggests that this reaction is driven by the ability of the Au NP to stabilize the developing hydride.

Haruta's group originally showed that H_2 activation rates track with the number of metal−support interface sites and determined a consistent turnover frequency for H_2−D_2 equilibration across a large range of particle sizes assuming that the active sites were at the MSI.[90] Takeda and co-worker's DFT study found a similar decrease in the activation barrier for H_2 dissociation at the MSI on Au/TiO_2. This study also suggested H_2 dissociation through an $O^{2−}$−H^+−$H^−$−Au pathway at the Au/TiO_2 interface was energetically favored compared to the Au−H−H−Au pathway.[99] In a different study using H_2−D_2 exchange reactions, Nakamura et al. also propose the $Au^{\delta+}$−$O^{\delta−}$−Ti sites at the Au/TiO_2 interface to be the active sites for H_2 dissociation.[155] The strong evidence for heterolytic H_2 activation reported here provides a clear mechanistic understanding of these reports.

Many other supported metal catalyst systems contain soft Lewis acids in close proximity to weak Brønsted bases, yet undergo homolytic H_2 activation on the metal. This is likely due to the electronic structure and high electronegativity of Au. Dissociative chemisorption, which is analogous to oxidative addition in transition metal complexes, requires a formal two-electron oxidation of the metal NP. The high electronegativity of Au, combined with the particularly stable full d-band, make Au the most noble metal and increase the thermodynamic and kinetic barriers for dissociative chemisorption. The heterolytic pathway does not require a formal oxidation of the metal, and thus appears to be the favored H_2 activation pathway for Au.

CONCLUSIONS

Kinetic experiments for H_2 oxidation over Au/TiO_2 and Au/Al_2O_3 catalysts show unexpectedly high reaction orders for H_2 and strong reaction inhibition by water physisorbed on the support. Combined with previous results for water-assisted CO oxidation on Au catalysts, this study shows that water drastically improves PrOx performance by promoting CO oxidation and inhibiting the undesirable H_2 oxidation reaction. However, the reaction kinetics are inconsistent with the traditional model for homolytic H_2 adsorption and subsequent hydrogenation of oxygen moieties exclusively on metal sites.

DFT studies using a rutile TiO_2(110)-supported Au nanorod model indicate that H_2 activation is most facile across the MSI. Surprisingly, the DFT model shows this to occur through a heterolytic H−H dissociation pathway, resulting in a proton adsorbed on a support hydroxyl group and a formal hydride adsorbed on the Au. This pathway does not require the formal oxidation of Au associated with the traditional homolytic activation mechanism that is commonly seen on other metals. Infrared spectroscopy experiments during H_2 adsorption on a deuterated Au/TiO_2 catalyst showed H−D scrambling with the metal oxide, lending further support for the heterolytic activation pathway. The experimental reaction kinetics were also consistent with the heterolytic H_2 activation model, and showed that the water

poisoning of H_2 oxidation was largely due to active site blocking.

The reaction network provided important fundamental insights into the nature of the catalysis. Protons near the MSI were calculated to be more stable than formal Au hydrides; yet, the MSI protons play the dominant role in fastest pathways for water formation. From the perspective of omnipresent transition state scaling or Brønsted–Evans–Polanyi relationships, this finding is counterintuitive. This system provides an example of how different types of chemistries (in this case metal sites with weak Brønsted acid/base chemistry) can be combined to overcome scaling relations and lead to significantly faster catalysis.

■ ASSOCIATED CONTENT

Ⓢ Supporting Information

The Supporting Information is available free of charge on the ACS Publications website at DOI: 10.1021/jacs.8b04991.

> O_2 reaction order plots; water effects on CO oxidation on Au/TiO_2; homolytic and heterolytic H_2 activation mechanisms and rate law derivations; effect of compressive strain and surface hydroxylation on the reactivity of Au/TiO_2; calculated energetics and configurations for each elementary step (PDF)

■ AUTHOR INFORMATION

Corresponding Author

*Bert.chandler@trinity.edu

ORCID Ⓘ

Lars C. Grabow: 0000-0002-7766-8856
Bert D. Chandler: 0000-0002-8621-0361

Author Contributions

§T. Whittaker and K. B. Sravan Kumar contributed equally to this work.

Notes

The authors declare no competing financial interest.

■ ACKNOWLEDGMENTS

■ REFERENCES

(1) Neef, H. J. International overview of hydrogen and fuel cell research. *Energy* **2009**, *34* (3), 327–333.

(2) Liu, K.; Song, C.; Subramani, V. *Hydrogen and Syngas Production and Purification Technologies*; John Wiley & Sons, Inc., 2010.

(3) Integrated Pollution Prevention and Control:. European Commission: 2007; p http://eippcb.jrc.ec.europa.eu/reference/BREF/lvic_aaf.pdf.

(4) Landon, P.; Ferguson, J.; Solsona, B. E.; Garcia, T.; Al-Sayari, S.; Carley, A. F.; Herzing, A. A.; Kiely, C. J.; Makkee, M.; Moulijn, J. A.; Overweg, A.; Golunski, S. E.; Hutchings, G. J. Selective oxidation of CO in the presence of H2, H2O and CO2 utilising Au/α-Fe2O3 catalysts for use in fuel cells. *J. Mater. Chem.* **2006**, *16* (2), 199–208.

(5) Schumacher, B.; Denkwitz, Y.; Plzak, V.; Kinne, M.; Behm, R. J. Kinetics, mechanism, and the influence of H2 on the CO oxidation reaction on a Au/TiO2 catalyst. *J. Catal.* **2004**, *224* (2), 449–462.

(6) Lakshmanan, P.; Park, J.; Park, E. Recent Advances in Preferential Oxidation of CO in H2 Over Gold Catalysts. *Catal. Surv. Asia* **2014**, *18* (2–3), 75–88.

(7) Bond, G. C.; Louis, C.; Thompson, D. T. *Catalysis by Gold*; Imperial College Press: London, 2006; Vol. 6, p 366.

(8) Haruta, M.; Kobayashi, T.; Sano, H.; Yamada, N. Novel gold catalysts for the oxidation of carbon monoxide at a temperature far below 0°C. *Chem. Lett.* **1987**, *16* (2), 405–8.

(9) Kung, M. C.; Davis, R. J.; Kung, H. H. Understanding Au-Catalyzed Low-Temperature CO Oxidation. *J. Phys. Chem. C* **2007**, *111* (32), 11767–11775.

(10) Valden, M.; Lai, X.; Goodman, D. W. Onset of catalytic activity of gold clusters on titania with the appearance of nonmetallic properties. *Science* **1998**, *281* (5383), 1647–1650.

(11) Green, I. X.; Tang, W.; Neurock, M.; Yates, J. T., Jr. Spectroscopic Observation of Dual Catalytic Sites During Oxidation of CO on a Au/TiO2 Catalyst. *Science* **2011**, *333*, 736–739.

(12) Widmann, D.; Behm, R. J. Activation of Molecular Oxygen and the Nature of the Active Oxygen Species for CO Oxidation on Oxide Supported Au Catalysts. *Acc. Chem. Res.* **2014**, *47* (3), 740–749.

(13) Saavedra, J.; Doan, H. A.; Pursell, C. J.; Grabow, L. C.; Chandler, B. D. The critical role of water at the gold-titania interface in catalytic CO oxidation. *Science* **2014**, *345* (6204), 1599–1602.

(14) Schubert, M. M.; Venugopal, A.; Kahlich, M. J.; Plzak, V.; Behm, R. J. Influence of H2O and CO2 on the selective CO oxidation in H2-rich gases over Au/α-Fe2O3. *J. Catal.* **2004**, *222* (1), 32–40.

(15) Denkwitz, Y.; Schumacher, B.; Kucerova, G.; Behm, R. J. Activity, stability, and deactivation behavior of supported Au/TiO2 catalysts in the CO oxidation and preferential CO oxidation reaction at elevated temperatures. *J. Catal.* **2009**, *267* (1), 78–88.

(16) Widmann, D.; Hocking, E.; Behm, R. J. On the origin of the selectivity in the preferential CO oxidation on Au/TiO2 - Nature of the active oxygen species for H2 oxidation. *J. Catal.* **2014**, *317*, 272–276.

(17) Hartadi, Y.; Behm, R.; Widmann, D. Competition of CO and H2 for Active Oxygen Species during the Preferential CO Oxidation (PROX) on Au/TiO2 Catalysts. *Catalysts* **2016**, *6* (2), 21.

(18) Rossignol, C.; Arrii, S.; Morfin, F.; Piccolo, L.; Caps, V.; Rousset, J.-L. Selective oxidation of CO over model gold-based catalysts in the presence of H2. *J. Catal.* **2005**, *230* (2), 476–483.

(19) Quinet, E.; Piccolo, L.; Morfin, F.; Avenier, P.; Diehl, F.; Caps, V.; Rousset, J.-L. On the mechanism of hydrogen-promoted gold-catalyzed CO oxidation. *J. Catal.* **2009**, *268* (2), 384–389.

(20) Kandoi, S.; Gokhale, A. A.; Grabow, L. C.; Dumesic, J. A.; Mavrikakis, M. Why Au and Cu are more selective than Pt for preferential oxidation of CO at low temperature. *Catal. Lett.* **2004**, *93* (1–2), 93–100.

(21) Nilekar, A. U.; Alayoglu, S.; Eichhorn, B.; Mavrikakis, M. Preferential CO Oxidation in Hydrogen: Reactivity of Core-Shell Nanoparticles. *J. Am. Chem. Soc.* **2010**, *132* (21), 7418–7428.

(22) Hibbitts, D.; Iglesia, E. Prevalence of Bimolecular Routes in the Activation of Diatomic Molecules with Strong Chemical Bonds (O2, NO, CO, N2) on Catalytic Surfaces. *Acc. Chem. Res.* **2015**, *48* (5), 1254–1262.

(23) Ojeda, M.; Zhan, B.-Z.; Iglesia, E. Mechanistic interpretation of CO oxidation turnover rates on supported Au clusters. *J. Catal.* **2012**, *285* (1), 92−102.

(24) Date, M.; Okumura, M.; Tsubota, S.; Haruta, M. Vital role of moisture in the catalytic activity of supported gold nanoparticles. *Angew. Chem., Int. Ed.* **2004**, *43* (16), 2129−2132.

(25) Fujitani, T.; Nakamura, I.; Haruta, M. Role of Water in CO Oxidation on Gold Catalysts. *Catal. Lett.* **2014**, *144* (9), 1475−1486.

(26) Date, M.; Haruta, M. Moisture Effect on CO Oxidation over Au/TiO2 Catalyst. *J. Catal.* **2001**, *201* (2), 221−224.

(27) Calla, J. T.; Davis, R. J. Influence of Dihydrogen and Water Vapor on the Kinetics of CO Oxidation over Au/Al2O3. *Ind. Eng. Chem. Res.* **2005**, *44* (14), 5403−5410.

(28) Calla, J. T.; Davis, R. J. Oxygen-exchange reactions during CO oxidation over titania- and alumina-supported Au nanoparticles. *J. Catal.* **2006**, *241* (2), 407−416.

(29) Calla, J. T.; Davis, R. J. Investigation of Alumina-Supported Au Catalyst for CO Oxidation by Isotopic Transient Analysis and X-ray Absorption Spectroscopy. *J. Phys. Chem. B* **2005**, *109* (6), 2307−2314.

(30) Saavedra, J.; Whittaker, T.; Chen, Z.; Pursell, C. J.; Rioux, R. M.; Chandler, B. D. Controlling activity and selectivity using water in the Au-catalysed preferential oxidation of CO in H2. *Nat. Chem.* **2016**, *8* (6), 584−589.

(31) Saavedra, J.; Pursell, C. J.; Chandler, B. D. CO Oxidation Kinetics over Au/TiO2 and Au/Al2O3 Catalysts: Evidence for a Common Water-Assisted Mechanism. *J. Am. Chem. Soc.* **2018**, *140*, 3712.

(32) Graham, T. On the relation of hydrogen to palladium. *J. Chem. Soc.* **1869**, *22*, 419−432.

(33) Draper, J. C. The separation by heat of arsenic from arseniuretted hydrogen in Marsh's test. *Sci. Am.* **1872**, *26*, 195−211.

(34) Boettger, R. On the preservation and properties of hydrogenated palladium. *Chem. Centr.* **1874**, 226−8.

(35) Oro, L. A.; Carmona, D.; Fraile, J. M. In *Hydrogenation Reactions*; Royal Society of Chemistry, 2006; pp 79−113.

(36) Zaera, F. The Surface Chemistry of Metal-Based Hydrogenation Catalysis. *ACS Catal.* **2017**, *7* (8), 4947−4967.

(37) Asatryan, R.; Ruckenstein, E. Dihydrogen Catalysis: A Remarkable Avenue in the Reactivity of Molecular Hydrogen. *Catal. Rev.: Sci. Eng.* **2014**, *56* (4), 403−475.

(38) Blaser, H.-U. The Development and Application of Industrially Viable Catalysts for the Selective Hydrogenation of Complex Molecules. *Top. Catal.* **2010**, *53* (15−18), 997−1001.

(39) Collman, J. P.; Hegedus, L. S.; Norton, J. R.; Finke, R. G. *Princilples and Applications of Organotransition Metal Chemistry*; University Science Books: Mill Valley, CA, 1987.

(40) Halpern, J. Catalytic activation of hydrogen in homogeneous, heterogeneous, and biological systems. *Adv. Catal.* **1959**, *11*, 301−70.

(41) Kubas, G. J. Fundamentals of H2 Binding and Reactivity on Transition Metals Underlying Hydrogenase Function and H2 Production and Storage. *Chem. Rev. (Washington, DC, U. S.)* **2007**, *107* (10), 4152−4205.

(42) Paal, Z.; Menon, P. G. Hydrogen effects in metal catalysts. *Catal. Rev.: Sci. Eng.* **1983**, *25* (2), 229−324.

(43) Christmann, K. Some general aspects of hydrogen chemisorption on metal surfaces. *Prog. Surf. Sci.* **1995**, *48* (1−4), 15−26.

(44) Joubert, J.; Salameh, A.; Krakoviack, V.; Delbecq, F.; Sautet, P.; Coperet, C.; Basset, J. M. Heterolytic Splitting of H2 and CH4 on γ-Alumina as a Structural Probe for Defect Sites. *J. Phys. Chem. B* **2006**, *110* (47), 23944−23950.

(45) Wischert, R.; Coperet, C.; Delbecq, F.; Sautet, P. Optimal Water Coverage on Alumina: A Key to Generate Lewis Acid-Base Pairs that are Reactive Towards the C-H Bond Activation of Methane. *Angew. Chem., Int. Ed.* **2011**, *50* (14), 3202−3205.

(46) Wischert, R.; Laurent, P.; Coperet, C.; Delbecq, F.; Sautet, P. γ-Alumina: The Essential and Unexpected Role of Water for the Structure, Stability, and Reactivity of Defect Sites. *J. Am. Chem. Soc.* **2012**, *134* (35), 14430−14449.

(47) Boudart, M.; Delbouille, A.; Derouane, E. G.; Indovina, V.; Walters, A. B. Activation of hydrogen at 78.deg.K on paramagnetic centers of magnesium oxide. *J. Am. Chem. Soc.* **1972**, *94* (19), 6622−6630.

(48) Lubitz, W.; Ogata, H.; Ruediger, O.; Reijerse, E. Hydrogenases. *Chem. Rev. (Washington, DC, U. S.)* **2014**, *114* (8), 4081−4148.

(49) Gloaguen, F.; Rauchfuss, T. B. Small molecule mimics of hydrogenases: hydrides and redox. *Chem. Soc. Rev.* **2009**, *38* (1), 100−108.

(50) Stephan, D. W. Frustrated Lewis pairs: a new strategy to small molecule activation and hydrogenation catalysis. *Dalton Transactions* **2009**, No. 17, 3129−3136.

(51) Greb, L.; Ona-Burgos, P.; Schirmer, B.; Grimme, S.; Stephan, D. W.; Paradies, J. Metal-free Catalytic Olefin Hydrogenation: Low-Temperature H2 Activation by Frustrated Lewis Pairs. *Angew. Chem., Int. Ed.* **2012**, *51* (40), 10164−10168.

(52) Stephan, D. W.; Erker, G. Frustrated Lewis Pair Chemistry: Development and Perspectives. *Angew. Chem., Int. Ed.* **2015**, *54* (22), 6400−6441.

(53) Chernichenko, K.; Madarasz, A.; Papai, I.; Nieger, M.; Leskelae, M.; Repo, T. A frustrated-Lewis-pair approach to catalytic reduction of alkynes to cis-alkenes. *Nat. Chem.* **2013**, *5* (8), 718−723.

(54) Kumar, G.; Tibbitts, L.; Newell, J.; Panthi, B.; Mukhopadhyay, A.; Rioux, R. M.; Pursell, C. J.; Janik, M.; Chandler, B. D. Evaluating differences in the active-site electronics of supported Au nanoparticle catalysts using Hammett and DFT studies. *Nat. Chem.* **2018**, *10*, 268.

(55) Kresse, G.; Furthmuller, J. Efficiency of ab-initio total energy calculations for metals and semiconductors using a plane-wave basis set. *Comput. Mater. Sci.* **1996**, *6* (1), 15−50.

(56) Kresse, G.; Furthmueller, J. Efficient iterative schemes for ab initio total-energy calculations using a plane-wave basis set. *Phys. Rev. B: Condens. Matter Mater. Phys.* **1996**, *54* (16), 11169−11186.

(57) Kresse, G.; Hafner, J. Ab initio molecular dynamics of liquid metals. *Phys. Rev. B: Condens. Matter Mater. Phys.* **1993**, *47* (1), 558−61.

(58) Wellendorff, J.; Lundgaard, K. T.; Moegelhoej, A.; Petzold, V.; Landis, D. D.; Noerskov, J. K.; Bligaard, T.; Jacobsen, K. W. Density functionals for surface science: exchange-correlation model development with Bayesian error estimation. *Phys. Rev. B: Condens. Matter Mater. Phys.* **2012**, *85* (23), 235149/1−235149/23.

(59) Kresse, G.; Joubert, D. From ultrasoft pseudopotentials to the projector augmented-wave method. *Phys. Rev. B: Condens. Matter Mater. Phys.* **1999**, *59* (3), 1758−1775.

(60) Bloechl, P. E. Projector augmented-wave method. *Phys. Rev. B: Condens. Matter Mater. Phys.* **1994**, *50* (24), 17953−79.

(61) Duan, Z.; Henkelman, G. CO Oxidation at the Au/TiO2 Boundary: The Role of the Au/Ti5c Site. *ACS Catal.* **2015**, *5* (3), 1589−1595.

(62) Dudarev, S. L.; Botton, G. A.; Savrasov, S. Y.; Humphreys, C. J.; Sutton, A. P. Electron-energy-loss spectra and the structural stability of nickel oxide: An LSDA+U study. *Phys. Rev. B: Condens. Matter Mater. Phys.* **1998**, *57* (3), 1505−1509.

(63) Hu, Z.; Metiu, H. Choice of U for DFT+U Calculations for Titanium Oxides. *J. Phys. Chem. C* **2011**, *115* (13), 5841−5845.

(64) Tripkovic, V.; Cerri, I.; Nagami, T.; Bligaard, T.; Rossmeisl, J. Platinum redispersion on metal oxides in low temperature fuel cells. *Phys. Chem. Chem. Phys.* **2013**, *15* (9), 3279−3285.

(65) Hellwege, K.; Hellwege, A. Structure Data of Elements and Intermetallic Phases. *Landolt-Bornstein, New Series* **1971**.

(66) Bader, R. F. W. *Atoms in Molecules: A Quantum Theory*; Oxford Univ. Press: 1994.

(67) Henkelman, G.; Arnaldsson, A.; Jónsson, H. A fast and robust algorithm for Bader decomposition of charge density. *Comput. Mater. Sci.* **2006**, *36* (3), 354−360.

(68) Tang, W.; Sanville, E.; Henkelman, G. A grid-based Bader analysis algorithm without lattice bias. *J. Phys.: Condens. Matter* **2009**, *21* (8), 084204.

(69) Pan, J. M.; Maschhoff, B.; Diebold, U.; Madey, T. E. *Interaction of Water, Oxygen, and Hydrogen with TiO2(110) Surfaces Having Different Defect Densities*; 1992; Vol. 10, pp 2470−2476.

(70) Mavrikakis, M.; Hammer, B.; Norskov, J. K. Effect of strain on the reactivity of metal surfaces. *Phys. Rev. Lett.* **1998**, *81* (13), 2819−2822.

(71) Laursen, S.; Linic, S. Geometric and electronic characteristics of active sites on TiO2-supported Au nano-catalysts: insights from first principles. *Phys. Chem. Chem. Phys.* **2009**, *11* (46), 11006−11012.

(72) Sivadinarayana, C.; Choudhary, T. V.; Daemen, L. L.; Eckert, J.; Goodman, D. W. The Nature of the Surface Species Formed on Au/TiO2 during the Reaction of H2 and O2: An Inelastic Neutron Scattering Study. *J. Am. Chem. Soc.* **2004**, *126* (1), 38−39.

(73) Saavedra, J.; Pursell, C. J.; Chandler, B. D. CO Oxidation Kinetics over Au/TiO2 and Au/Al2O3 Catalysts: Evidence for a Common Water-Assisted Mechanism. *J. Am. Chem. Soc.* **2018**, *140* (10), 3712−3723.

(74) Rodriguez, J. A.; Ma, S.; Liu, P.; Hrbek, J.; Evans, J.; Perez, M. Activity of CeOx and TiOx Nanoparticles Grown on Au(111) in the Water-Gas Shift Reaction. *Science (Washington, DC, U. S.)* **2007**, *318* (5857), 1757−1760.

(75) Boudart, M.; Collins, D. M.; Hanson, F. V.; Spicer, W. E. Reactions between hydrogen and oxygen on platinum at low and high pressures: a comparison. *J. Vac. Sci. Technol.* **1977**, *14* (1), 441−3.

(76) Engel, T.; Kuipers, H. A molecular-beam investigation of the reaction H2 + 12O2 → H2O on Pd(111). *Surf. Sci.* **1979**, *90* (1), 181−196.

(77) Gdowski, G. E.; Madix, R. J. The kinetics and mechanism of the hydrogen-oxygen reaction on Pt(S)−[9(111) × (100)]. *Surf. Sci.* **1982**, *119* (2), 184−206.

(78) Gland, J. L.; Fisher, G. B.; Kollin, E. B. Hydrogen-oxygen reaction over the Pt(111) surface: transient titration of adsorbed oxygen with hydrogen *J. Catal.* **1982**, *77*, 263−278.

(79) Hanson, F. V.; Boudart, M. The reaction between H2 and O2 over supported platinum catalysts. *J. Catal.* **1978**, *53* (1), 56−67.

(80) Pacia, N.; Dumesic, J. A. Oxidation of hydrogen on polycrystalline platinum studied by molecular beam reactive scattering. *J. Catal.* **1976**, *41* (1), 155−67.

(81) Padowitz, D. F.; Sibener, S. J. Kinetics of hydrogen oxidation to water on the Rh(111) surface using multiple source modulated molecular beam techniques. *Surf. Sci.* **1991**, *254* (1), 125−143.

(82) Hussain, A.; Gracia, J.; Nieuwenhuys, B. E.; Niemantsverdriet, J. W. Explicit Roles of Au and TiO2 in a Bifunctional Au/TiO2 Catalyst for the Water-Gas Shift Reaction: A DFT Study. *ChemCatChem* **2013**, *5* (8), 2479−2488.

(83) Sun, K.; Kohyama, M.; Tanaka, S.; Takeda, S. Reaction Mechanism of the Low-Temperature Water-Gas Shift Reaction on Au/TiO2 Catalysts. *J. Phys. Chem. C* **2017**, *121* (22), 12178−12187.

(84) Carrasco, J.; Klimeš, J.; Michaelides, A. The role of van der Waals forces in water adsorption on metals. *J. Chem. Phys.* **2013**, *138* (2), 024708.

(85) Pan, M.; Pozun, Z. D.; Yu, W.-Y.; Henkelman, G.; Mullins, C. B. Structure Revealing H/D Exchange with Co-Adsorbed Hydrogen and Water on Gold. *J. Phys. Chem. Lett.* **2012**, *3* (14), 1894−1899.

(86) Corem, G.; Kole, P. R.; Zhu, J.; Kravchuk, T.; Manson, J. R.; Alexandrowicz, G. Ordered H2O Structures on a Weakly Interacting Surface: A Helium Diffraction Study of H2O/Au(111). *J. Phys. Chem. C* **2013**, *117* (45), 23657−23663.

(87) Velasco-Velez, J.-J.; Wu, C. H.; Pascal, T. A.; Wan, L. F.; Guo, J.; Prendergast, D.; Salmeron, M. The structure of interfacial water on gold electrodes studied by x-ray absorption spectroscopy. *Science (Washington, DC, U. S.)* **2014**, *346* (6211), 831−834.

(88) Stacchiola, D.; Park, J. B.; Liu, P.; Ma, S.; Yang, F.; Starr, D. E.; Muller, E.; Sutter, P.; Hrbek, J. Water Nucleation on Gold: Existence of a Unique Double Bilayer. *J. Phys. Chem. C* **2009**, *113* (34), 15102−15105.

(89) Ikemiya, N.; Gewirth, A. A. Initial Stages of Water Adsorption on Au Surfaces. *J. Am. Chem. Soc.* **1997**, *119* (41), 9919−9920.

(90) Fujitani, T.; Nakamura, I.; Akita, T.; Okumura, M.; Haruta, M. Hydrogen Dissociation by Gold Clusters. *Angew. Chem., Int. Ed.* **2009**, *48* (50), 9515−9518.

(91) Panthi, B.; Mukhopadhyay, A.; Tibbitts, L.; Saavedra, J.; Pursell, C. J.; Rioux, R. M.; Chandler, B. D. Using Thiol Adsorption on Supported Au Nanoparticle Catalysts To Evaluate Au Dispersion and the Number of Active Sites for Benzyl Alcohol Oxidation. *ACS Catal.* **2015**, *5* (4), 2232−2241.

(92) Ward, T.; Delannoy, L.; Hahn, R.; Kendell, S.; Pursell, C. J.; Louis, C.; Chandler, B. D. Effects of Pd on Catalysis by Au: CO Adsorption, CO Oxidation, and Cyclohexene Hydrogenation by Supported Au and Pd-Au Catalysts. *ACS Catal.* **2013**, *3* (11), 2644−2653.

(93) Saavedra, J.; Powell, C.; Panthi, B.; Pursell, C. J.; Chandler, B. D. CO oxidation over Au/TiO2 catalyst: Pretreatment effects, catalyst deactivation, and carbonates production. *J. Catal.* **2013**, *307*, 37−47.

(94) Chandler, B. D.; Kendell, S.; Doan, H.; Korkosz, R.; Grabow, L. C.; Pursell, C. J. NaBr Poisoning of Au/TiO2 Catalysts: Effects on Kinetics, Poisoning Mechanism, and Estimation of the Number of Catalytic Active Sites. *ACS Catal.* **2012**, *2* (4), 684−694.

(95) Chandler, B. D.; Long, C. G.; Gilbertson, J. D.; Vijayaraghavan, G.; Stevenson, K. J.; Pursell, C. J. Improving Oxygen Activation Over Supported Au Catalysts Through the Controlled Preparation of Bimetallic Ni-Au Nanoparticles. *J. Phys. Chem. C* **2010**, *114*, 11498−11508.

(96) Long, C. G.; Gilbertson, J. D.; Vijayaraghavan, G.; Stevenson, K. J.; Pursell, C. J.; Chandler, B. D. Kinetic Evaluation of Highly Active Supported Gold Catalysts Prepared from Monolayer Protected Clusters: An Experimental Michaelis-Menten Approach for Determining the Oxygen Binding Constant During CO Oxidation Catalysis. *J. Am. Chem. Soc.* **2008**, *130*, 10103−10115.

(97) Naito, S.; Tanimoto, M. Mechanism of deuterium addition and exchange of propene over silica-supported gold and silver catalysts. *J. Chem. Soc., Faraday Trans. 1* **1988**, *84* (11), 4115−24.

(98) Bond, G. C.; Thompson, D. T. Catalysis by gold. *Catal. Rev.: Sci. Eng.* **1999**, *41*, 319−388.

(99) Sun, K.; Kohyama, M.; Tanaka, S.; Takeda, S. A Study on the Mechanism for H2 Dissociation on Au/TiO2 Catalysts. *J. Phys. Chem. C* **2014**, *118* (3), 1611−1617.

(100) Boronat, M.; Illas, F.; Corma, A. Active Sites for H2 Adsorption and Activation in Au/TiO2 and the Role of the Support. *J. Phys. Chem. A* **2009**, *113* (16), 3750−3757.

(101) Green, I. X.; Tang, W.; Neurock, M.; Yates, J. T. Spectroscopic Observation of Dual Catalytic Sites During Oxidation of CO on a Au/TiO2 Catalyst. *Science* **2011**, *333* (6043), 736.

(102) Molina, L. M.; Rasmussen, M. D.; Hammer, B. Adsorption of O2 and oxidation of CO at Au nanoparticles supported by TiO2(110). *J. Chem. Phys.* **2004**, *120* (16), 7673−7680.

(103) Wang, S.; Petzold, V.; Tripkovic, V.; Kleis, J.; Howalt, J. G.; Skulason, E.; Fernandez, E. M.; Hvolbaek, B.; Jones, G.; Toftelund, A.; Falsig, H.; Bjoerketun, M.; Studt, F.; Abild-Pedersen, F.; Rossmeisl, J.; Norskov, J. K.; Bligaard, T. Universal transition state scaling relations for (de)hydrogenation over transition metals. *Phys. Chem. Chem. Phys.* **2011**, *13* (46), 20760−20765.

(104) Grabow, L. C.; Hvolbæk, B.; Falsig, H.; Nørskov, J. K. Search Directions for Direct H2O2 Synthesis Catalysts Starting from Au12 Nanoclusters. *Top. Catal.* **2012**, *55* (5), 336−344.

(105) Kelly, C. A.; Rosseinsky, D. R. Estimates of hydride ion stability in condensed systems: energy of formation and solvation in aqueous and polar-organic solvents. *Phys. Chem. Chem. Phys.* **2001**, *3* (11), 2086−2090.

(106) Koch, D.; Manzhos, S. On the Charge State of Titanium in Titanium Dioxide. *J. Phys. Chem. Lett.* **2017**, *8* (7), 1593−1598.

(107) Prins, R. Hydrogen Spillover. Facts and Fiction. *Chem. Rev.* **2012**, *112* (5), 2714−2738.

(108) Claus, P. Heterogeneously catalysed hydrogenation using gold catalysts. *Appl. Catal., A* **2005**, *291* (1), 222−229.

(109) Baumgarten, E.; Wagner, R.; Lentes-Wagner, C. Reactivity of spillover hydrogen. Reactivity of unsaturated compounds. *J. Catal.* **1987**, *104* (2), 307−11.

(110) Miller, J. T.; Pei, S. Hydrogenation and deuterium exchange by spillover hydrogen of ethylbenzene adsorbed on H-USY zeolite. *Appl. Catal., A* **1998**, *168* (1), 1−7.

(111) Powell, C. D.; Daigh, A. W.; Pollock, M. N.; Chandler, B. D.; Pursell, C. J. CO Adsorption on Au/TiO2 Catalysts: Observations, Quantification, and Explanation of a Broad-Band Infrared Signal. *J. Phys. Chem. C* **2017**, *121* (44), 24541−24547.

(112) Bus, E.; Miller, J. T.; van Bokhoven, J. A. Hydrogen Chemisorption on Al2O3-Supported Gold Catalysts. *J. Phys. Chem. B* **2005**, *109* (30), 14581−14587.

(113) Joshi, A. M.; Delgass, W. N.; Thomson, K. T. H2 adsorption and H/D exchange on Au/TS-1 and Au/S-1 catalysts. *Top. Catal.* **2007**, *44* (1−2), 27−39.

(114) Stobinski, L.; Dus, R. Model of atomic hydrogen adsorption on thin gold film surface. *Vacuum* **1994**, *45* (2−3), 299−301.

(115) Stobinski, L.; Dus, R. Molecular hydrogen chemisorption on thin unsintered gold films deposited at low temperature. *Surf. Sci.* **1993**, *298* (1), 101−6.

(116) Sault, A. G.; Madix, R. J.; Campbell, C. T. Adsorption of oxygen and hydrogen on gold(110)-(1 × 2). *Surf. Sci.* **1986**, *169* (2−3), 347−56.

(117) Gatin, A. K.; Grishin, M. V.; Gurevich, S. A.; Dokhlikova, N. V.; Kirsankin, A. A.; Kozhevin, V. M.; Kolchenko, N. N.; Rostovshchikova, T. N.; Kharitonov, V. A.; Shub, B. R.; Yavsin, D. A. Interaction of hydrogen and oxygen on the surface of individual gold nanoparticles. *Russ. Chem. Bull.* **2014**, *63* (8), 1696−1702.

(118) Greeley, J.; Mavrikakis, M. Alloy catalysts designed from first principles. *Nat. Mater.* **2004**, *3* (11), 810−815.

(119) Greeley, J. Theoretical Heterogeneous Catalysis: Scaling Relationships and Computational Catalyst Design. *Annu. Rev. Chem. Biomol. Eng.* **2016**, *7*, 605−35.

(120) Hibbitts, D.; Neurock, M. Promotional effects of chemisorbed oxygen and hydroxide in the activation of C-H and O-H bonds over transition metal surfaces. *Surf. Sci.* **2016**, *650*, 210−220.

(121) Kumar, G.; Nikolla, E.; Linic, S.; Medlin, J. W.; Janik, M. J. Multicomponent Catalysts: Limitations and Prospects. *ACS Catal.* **2018**, *8* (4), 3202−3208.

(122) Wilson, N. M.; Priyadarshini, P.; Kunz, S.; Flaherty, D. W. Direct synthesis of H2O2 on Pd and AuxPd1 clusters: Understanding the effects of alloying Pd with Au. *J. Catal.* **2017**, *357*, 163−175.

(123) Flaherty, D. W. Direct Synthesis of H2O2 from H2 and O2 on Pd Catalysts: Current Understanding, Outstanding Questions, and Research Needs. *ACS Catal.* **2018**, *8* (2), 1520−1527.

(124) Pizzutilo, E.; Kasian, O.; Choi, C. H.; Cherevko, S.; Hutchings, G. J.; Mayrhofer, K. J. J.; Freakley, S. J. Electrocatalytic synthesis of hydrogen peroxide on Au-Pd nanoparticles: From fundamentals to continuous production. *Chem. Phys. Lett.* **2017**, *683*, 436−442.

(125) Lewis, R. J.; Edwards, J. K.; Freakley, S. J.; Hutchings, G. J. Solid Acid Additives as Recoverable Promoters for the Direct Synthesis of Hydrogen Peroxide. *Ind. Eng. Chem. Res.* **2017**, *56* (45), 13287−13293.

(126) Edwards, J. K.; Solsona, B.; Ntainjua, E.; Carley, A. F.; Herzing, A. A.; Kiely, C. J.; Hutchings, G. J. Switching Off Hydrogen Peroxide Hydrogenation in the Direct Synthesis Process. *Science (Washington, DC, U. S.)* **2009**, *323* (5917), 1037−1041.

(127) Carr, S. B.; Evans, R. M.; Brooke, E. J.; Wehlin, S. A. M.; Nomerotskaia, E.; Sargent, F.; Armstrong, F. A.; Phillips, S. E. V. Hydrogen activation by [NiFe]-hydrogenases. *Biochem. Soc. Trans.* **2016**, *44* (3), 863−868.

(128) Carr, S. B.; Phillips, S. E. V.; Evans, R. M.; Brooke, E. J.; Wehlin, S. A. M.; Nomerotskaia, E.; Armstrong, F. A.; Sargent, F. Hydrogen activation by [NiFe]-hydrogenases. *Biochem. Soc. Trans.* **2016**, *44* (3), 863−8.

(129) Dey, S.; Das, P. K.; Dey, A. Mononuclear iron hydrogenase. *Coord. Chem. Rev.* **2013**, *257* (1), 42−63.

(130) Shima, S.; Chen, D.; Xu, T.; Wodrich, M. D.; Fujishiro, T.; Schultz, K. M.; Kahnt, J.; Ataka, K.; Hu, X. Reconstitution of [Fe]-hydrogenase using model complexes. *Nat. Chem.* **2015**, *7* (12), 995−1002.

(131) Shima, S.; Fujishiro, T.; Kahnt, J.; Shima, S.; Chen, D.; Xu, T.; Wodrich, M. D.; Schultz, K. M.; Hu, X.; Wodrich, M. D.; Ataka, K. Reconstitution of [Fe]-hydrogenase using model complexes. *Nat. Chem.* **2015**, *7* (12), 995−1002.

(132) Brintzinger, H. H. Mechanisms of dihydrogen activation by zirconocene alkyl and hydride derivatives. A molecular orbital analysis of a direct hydrogen transfer reaction mode. *J. Organomet. Chem.* **1979**, *171* (3), 337−44.

(133) Dahlenburg, L.; Goetz, R. Iridium complexes with chiral and achiral β-aminophosphane ligands: Catalysts for > C=O hydrogenation and H/D exchange involving both homo- and heterolytic H2 activation. *Eur. J. Inorg. Chem.* **2004**, *2004* (4), 888−905.

(134) Dahlenburg, L.; Gotz, R. Functional phosphines XII. Heterolytic H2 cleavage and homogeneous C:O hydrogenation catalyzed by platinum metal β-aminophosphine complexes. *Inorg. Chem. Commun.* **2003**, *6* (5), 443−446.

(135) Flynn, S. R.; Metters, O. J.; Manners, I.; Wass, D. F. Zirconium-catalyzed imine hydrogenation via a frustrated Lewis pair mechanism. *Organometallics* **2016**, *35* (6), 847−850.

(136) Fong, H.; Moret, M.-E.; Lee, Y.; Peters, J. C. Heterolytic H2 Cleavage and Catalytic Hydrogenation by an Iron Metallaboratrane. *Organometallics* **2013**, *32* (10), 3053−3062.

(137) Gao, W.; Lv, H.; Zhang, X.; Lv, H.; Zhang, T.; Yang, Y.; Chung, L. W.; Zhang, X.; Zhang, T.; Wu, Y.-D. Nickel-catalyzed asymmetric hydrogenation of β-acylamino nitroolefins: an efficient approach to chiral amines. *Chem. Sci.* **2017**, *8* (9), 6419−false.

(138) Heshmat, M.; Privalov, T. Testing the nature of reaction coordinate describing interaction of H2 with carbonyl carbon, activated by Lewis acid complexation, and the Lewis basic solvent: A Born-Oppenheimer molecular dynamics study with explicit solvent. *J. Chem. Phys.* **2017**, *147* (9), 094302.

(139) Nisa, R. U.; Ayub, K. Mechanism of Zn(OTf)2 catalyzed hydroamination-hydrogenation of alkynes with amines: insight from theory. *New J. Chem.* **2017**, *41* (12), 5082−5090.

(140) Rawat, K. S.; Mahata, A.; Choudhuri, I.; Pathak, B. Catalytic Hydrogenation of CO2 by Manganese Complexes: Role of π-Acceptor Ligands. *J. Phys. Chem. C* **2016**, *120* (30), 16478−16488.

(141) Teets, T. S.; Labinger, J. A.; Bercaw, J. E. A Thermodynamic Analysis of Rhenium(I)-Formyl C-H Bond Formation via Base-Assisted Heterolytic H2 Cleavage in the Secondary Coordination Sphere. *Organometallics* **2013**, *32* (19), 5530−5545.

(142) Pearson, R. G. The transition-metal-hydrogen bond. *Chem. Rev.* **1985**, *85* (1), 41−9.

(143) Aldridge, S.; Downs, A. J. Hydrides of the main-group metals. New variations on an old theme. *Chem. Rev. (Washington, DC, U. S.)* **2001**, *101* (11), 3305−3365.

(144) Omotoso, T. O.; Baek, B.; Grabow, L. C.; Crossley, S. P. Experimental and First-Principles Evidence for Interfacial Activity of Ru/TiO2 for the Direct Conversion of m-Cresol to Toluene. *ChemCatChem* **2017**, *9* (14), 2612.

(145) Nelson, R. C.; Baek, B.; Ruiz, P.; Goundie, B.; Brooks, A.; Wheeler, M. C.; Frederick, B. G.; Grabow, L. C.; Austin, R. N. Experimental and Theoretical Insights into the Hydrogen-Efficient Direct Hydrodeoxygenation Mechanism of Phenol over Ru/TiO2. *ACS Catal.* **2015**, *5* (11), 6509−6523.

(146) Koso, S.; Nakagawa, Y.; Tomishige, K. Mechanism of the hydrogenolysis of ethers over silica-supported rhodium catalyst modified with rhenium oxide. *J. Catal.* **2011**, *280* (2), 221−229.

(147) Camacho-Bunquin, J.; Ferrandon, M.; Das, U.; Dogan, F.; Liu, C.; Larsen, C.; Platero-Prats, A. E.; Curtiss, L. A.; Hock, A. S.; Miller, J. T.; Nguyen, S. T.; Marshall, C. L.; Delferro, M.; Stair, P. C. Supported Aluminum Catalysts for Olefin Hydrogenation. *ACS Catal.* **2017**, *7* (1), 689−694.

(148) Ren, D.; He, L.; Yu, L.; Ding, R.-S.; Liu, Y.-M.; Cao, Y.; He, H.-Y.; Fan, K.-N. An Unusual Chemoselective Hydrogenation of

Quinoline Compounds Using Supported Gold Catalysts. *J. Am. Chem. Soc.* **2012**, *134* (42), 17592−17598.

(149) Fiorio, J. L.; Gonçalves, R. V.; Teixeira-Neto, E.; Ortuño, M. A.; López, N.; Rossi, L. M. Accessing Frustrated Lewis Pair Chemistry through Robust Gold@N-Doped Carbon for Selective Hydrogenation of Alkynes. *ACS Catal.* **2018**, *8* (4), 3516−3524.

(150) Fiorio, J. L.; López, N.; Rossi, L. M. Gold−Ligand-Catalyzed Selective Hydrogenation of Alkynes into cis-Alkenes via H2 Heterolytic Activation by Frustrated Lewis Pairs. *ACS Catal.* **2017**, *7* (4), 2973−2980.

(151) Luza, L.; Rambor, C. P.; Gual, A.; Alves Fernandes, J.; Eberhardt, D.; Dupont, J. Revealing Hydrogenation Reaction Pathways on Naked Gold Nanoparticles. *ACS Catal.* **2017**, *7* (4), 2791−2799.

(152) Cano, I.; Chapman, A. M.; Urakawa, A.; van Leeuwen, P. W. N. M. Air-Stable Gold Nanoparticles Ligated by Secondary Phosphine Oxides for the Chemoselective Hydrogenation of Aldehydes: Crucial Role of the Ligand. *J. Am. Chem. Soc.* **2014**, *136* (6), 2520−2528.

(153) Almora-Barrios, N.; Cano, I.; van Leeuwen, P. W. N. M.; López, N. Concerted Chemoselective Hydrogenation of Acrolein on Secondary Phosphine Oxide Decorated Gold Nanoparticles. *ACS Catal.* **2017**, *7* (6), 3949−3954.

(154) Pearson, R. G. Hard and soft acids and bases. *J. Am. Chem. Soc.* **1963**, *85* (22), 3533−9.

(155) Nakamura, I.; Mantoku, H.; Furukawa, T.; Fujitani, T. Active Sites for Hydrogen Dissociation over TiOx/Au(111) Surfaces. *J. Phys. Chem. C* **2011**, *115* (32), 16074−16080.